

Intelligent Physical Attack Against Mobile Robots With Obstacle-Avoidance

Yushan Li, *Student Member, IEEE*, Jianping He, *Senior Member, IEEE*, Cailian Chen, *Member, IEEE*
and Xinping Guan, *Fellow, IEEE*

Abstract—The security issue of mobile robots has attracted considerable attention in recent years. In this paper, we propose an intelligent physical attack to trap mobile robots into a preset position by learning the obstacle-avoidance mechanism from external observation. The salient novelty of our work lies in revealing the possibility that physical-based attacks with intelligent and advanced design can present real threats, while without prior knowledge of the system dynamics or access to the internal system. This kind of attack cannot be handled by countermeasures in traditional cyberspace security. To practice, the cornerstone of the proposed attack is to actively explore the complex interaction characteristic of the victim robot with the environment, and learn the obstacle-avoidance knowledge exhibited in the limited observations of its behaviors. Then, we propose shortest-path and hands-off attack algorithms to find efficient attack paths from the tremendous motion space, achieving the driving-to-trap goal with low costs in terms of path length and activity period, respectively. The convergence of the algorithms is proved and the attack performance bounds are further derived. Extensive simulations and real-life experiments illustrate the effectiveness of the proposed attack, beckoning future investigation for the new physical threats and defense on robotic systems.

Index Terms—Intelligent attack, mobile robots, intentional learning, obstacle-avoidance.

I. INTRODUCTION

With integrated communication, computation and control to support the operations in the physical world, the mobile robots can be seen as a typical cyber-physical system (CPS), attracting extensive attention thanks to their excellent flexibility and scalability. From UAVs to UGVs, either single or multiple coordinated, mobile robots are becoming more and more pervasive in industrial and military fields, e.g., logistics transportation, environment exploration, surveillance and reconnaissance. With this ever-increasing popularity, their security becomes critical yet imperatively challenging [1], given numerous possible malicious or unanticipated behaviors.

This paper investigates a novel intelligent physical attack against mobile robots without relying on any prior knowledge. The ultimate goal of the attacker is to learn the obstacle-avoidance mechanism of a mobile robot from external observation, and then leverage it to fool the target robot into a preset trap. This problem is inspired by the intrinsic interaction

nature of a robot with the physical environment and its security issues. On the one hand, prior works concerning the security of mobile robots are mainly developed from the perspective of cyberspace [2], [3], while physical attacks are less noticed yet also critically important. It is universally needed for mobile robots in the real world to interact with the physical environment [4]. By disguising as an obstacle and physically approaching a robot, the resulting obstacle-avoidance behavior is inevitable, providing support to trap the robot. On the other hand, numerous defense techniques assume possible attacks are powerful beforehand [5], [6], obtaining robust security performance while incurring more costs, e.g., hardware computation burdens. Indeed, if an attack is figured to be almost impossible to launch, then there is no need to design sophisticated countermeasures along with performance degradations, better guiding the systems defense design.

Despite some similar features between the attack problem in this paper and classic pursuit-evasion [7]–[9] and herding problems [10]–[12], we point out there are still major differences in their application scenarios and basic model formulation. First, the physical attack here is not purely about controlling a robot to capture or track the victim robot, but making the victim robot move to a preset deterministic position. Second, unlike the aforementioned works that usually assume complete or partial knowledge about interaction models is available, the attacker here has no prior knowledge about the victim robot. It needs to actively learn the necessary obstacle-avoidance knowledge first, making the attack more generalizable and applicable to a majority of obstacle-avoidance mechanisms, which is a significant and unique component of this paper. Besides, compared with directly intercepting (e.g., missile guidance [13]) or decoding-and-manipulating the communication messages (especially when the control-communication is protected with strong encryption [14], [15]), the proposed physical attack is more feasible, stealthy and economically viable, presenting serious threats.

To systematically design and evaluate the intelligent physical attacks on mobile robots, three major challenges must be addressed. First, the attacker is unaware of the prerequisite information that supports the attack (like the obstacle detection range and goal position), making it an impediment to formulating the attack model by traditional techniques, e.g., parameter identification and model predictive control. Second, the attacker and victim robots are mutually influenced in the motion space, incurring difficulties to find the feasible solution space that meets the attack requirements. Third, even if a feasible solution space is found, it is hard to optimize strategy

The authors are with the Department of Automation, Shanghai Jiao Tong University, Shanghai 200240, China; Key Laboratory of System Control and Information Processing, Ministry of Education of China, Shanghai 200240, China; Shanghai Engineering Research Center of Intelligent Control and Management, Shanghai 200240, China. E-mail address: {yushan_li, jphe, cailianchen, xpguan}@sjtu.edu.cn.

designs to achieve the final purpose with low attack costs.

This paper is an extension of the preliminary work presented in [16], providing a detailed and rigorous treatment of model learning, attack design and performances analysis, as well as significant novel simulation results. The main contributions of this paper are as follows:

- We investigate the possibility of achieving an intelligent and advanced physical attack against mobile robots, merely utilizing external observations and not relying on any prior information of the system dynamics. Taking the universal obstacle-avoidance mechanism as the attack interface, we provide a systematic attack scheme including knowledge-learning and attack implementation.
- We propose an intentional excitation based learning approach to acquire the obstacle-avoidance knowledge. By characterizing the obstacle-avoidance behaviors and disguising the attacker as an obstacle, we demonstrate how to excite various avoidance reactions of the victim robot. Based on observations over this process, we establish the featured data pairs that reflect the underlying mechanism and further regress it by learning-based methods.
- We design two driving-to-trap attack algorithms by taking the attack path length and activity period as the objectives, respectively. We prove the convergence of the attack algorithms from the perspective of the descent search. The performance bounds of the algorithms are further derived concerning the optimal cost in theory. Extensive simulations and real-life experiments are conducted to illustrate the effectiveness of the proposed attack.

In a larger sense, this paper reveals the vulnerability of system security from external observation and excitation. As the obstacle-avoidance behavior is indispensable for a mobile robot to interact with the environment, the proposed attack is hard to defend when the robot has no prior knowledge about the malicious behavior, where the attacker is not always consistently but intermittently active during the process. Therefore, our work lays the foundation to explore more potential and advanced attacks against mobile robots from physical aspects, and provides deeper insight to guide the defense design in the future.

The rest of this paper is organized as follows. To begin with, Section II presents an overview of the relevant literature. In Section III, the kinematics and obstacle-avoidance modeling for both holonomic and non-holonomic mobile robots are introduced. The learning scheme for the obstacle-avoidance mechanism is proposed in Section IV. Section V presents the attack strategies with performance analysis. Simulations and experiments are shown in Section VI and Section VII, respectively. Finally, Section VIII concludes this paper. A roadmap of the main results of this paper is shown in Fig. 1.

II. RELATED WORK

There are mainly two related topics: CPS security and obstacle-avoidance mechanism. Given the richness of both fields, a brief overview of some representative works is given.

CPS security. The security shows the ability of a system to govern malicious behaviors or unanticipated events [17].

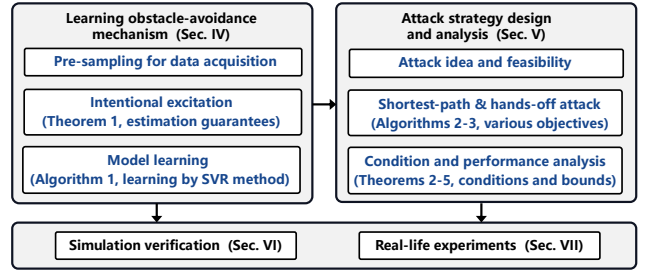


Fig. 1. Roadmap of the main results in this paper.

In the literature, attacks against mobile robots are mainly from cyberspace, and they can be roughly divided into three categories: denial of service (DoS), replay, and deception attacks [2]. In these attacks, communication channels are jammed/disrupted [18], or the control data and measurements are compromised/altered [19], and thus compromising the systems in critical and adversarial scenarios. Many efforts have been devoted to designing corresponding countermeasures. For instance, [6] characterized the undetectable and unidentifiable attacks and designed corresponding detection filters. [20] considered the secure estimation problem where the set of attacked nodes can change with time. The motion synchronization methods were developed for robot formation considering the presence of robot malfunctions [21], [22] or undesirable formation variation [23], [24]. A group of robots were deployed to herd an adversarial aerial attacker to defend safety-critical infrastructure in [25]. However, most existing research relied on the assumption that the attacker has some knowledge or can access the robot system. For example, malicious agents have knowledge of the system structure or nodes' states [5], or the packets transmitted over the network are corrupted [26], [27]. These assumptions may no longer hold given the cryptographic solutions in practice.

In recent years, stealthy physical attacks emerged and presented real threats, where the physical components were targeted to compromise or even destroy the system. For instance, the GPS sensor readings can be disturbed by GPS spoofing attack [28], [29]. Designed acoustic noises can alter gyroscopic sensor data, leading to drone crashes [30]. Even the important values stored in memory (e.g., EEPROM, Flash memory) can be corrupted by heating a memory cell while the device is without any damage [31]. Compared with cyber attacks, these physical attacks have a wider range of applicability, while the traditional detection techniques from the computer security community are usually not effective in handling them [1]. Note that these emerging physical attacks are still elementary and not sufficiently intelligent. For instance, the attacks were designed against a specific transducer by utilizing its sensing mechanism, and cannot be generalized. In addition, these physical attacks aiming to disturb the system performance were designed with an “open-loop” flavor and without sophisticated control design, which motivates this work to investigate possible physical attacks with intelligence.

Obstacle-avoidance mechanism. Obstacle-avoidance is the major interface for mobile robots to interact with the outside environment. Numerous methods have been developed in the

TABLE I
NOTATION DEFINITIONS

Symbol	Definition
R_a	the abbreviated form of the attack robot
R_v	the abbreviated form of the victim robot
f	the obstacle-avoidance mechanism
\mathcal{J}	the observed dataset for learning the knowledge about f
p_ϑ	the position variable. $\vartheta = a, v, g, t, e$ represent the position of R_a, R_v , the task goal, the preset trap, and the attack entry point, respectively
\mathcal{T}_ϑ	the trajectory variable. $\vartheta = g, a, m$ represent the ideal trajectory of R_v to p_g without being attacked, the ideal attack trajectory from p_e to p_t , and the instantaneous motion direction trajectory of a robot, respectively
\mathcal{A}_ϑ	the area variable, representing a set of specific positions
(D, α)	the obstacle-avoidance detection range, where D is the radius and α is the angle range
$d(p_1, p_2)$	the distance between p_1 and p_2 , i.e., $\ p_2 - p_1\ _2$
$d_T(\mathcal{T}_\vartheta, p)$	the minimal distance from a position p to \mathcal{T}_ϑ
$I_T(\mathcal{T}_\vartheta, p)$	the indicative function to judge whether p is on \mathcal{T}_ϑ

literature, for example, potential field based approach [32], genetic algorithm based approach [33], fuzzy logic based approach [34], neural network based approach [35], etc (see [36], [37] for a detailed review). According to their algorithm characteristic, similar to [38], we divide these algorithms into two main types: deterministic (e.g., artificial potential method, learning-based method) and search-based (e.g., dynamic window approach, genetic approach, evolutionary algorithm). The former is determined-model driven¹ and the solution for the current situation is unique and found quickly. The key idea of the latter one is to search for all feasible solutions and select the best one according to an evaluation function, which is time-consuming. No matter what obstacle-avoidance method is used, the essence of circumventing the obstacle with certain trajectory adjustment towards its goal is identical and directly leaks to external observation. This nature is captured and leveraged in our attack design.

In summary, it remains an open yet critical issue to investigate what kind of intelligent and generalized attack is available from the physical side, while without prior knowledge about the system.

III. PRELIMINARY AND PROBLEM FORMULATION

In this section, we first introduce some basics about the kinematics of a mobile robot. The motion dynamics of both holonomic and non-holonomic mobile robots are presented. Following this, we show what an important role the obstacle-avoidance plays. At last, our problem of interest is formulated. Some important notation and definitions are given in Table I.

A. Motion Control for Mobile Robots

It should be mentioned that there are generally two kinds of mobile robots: non-holonomic (car-like wheeled mobile agents, unicycles, etc.) and holonomic. Although the former one appears more common in daily life, their instantaneous

movement is restricted laterally [39], making the control more challenging than that of the latter kind.

For a non-holonomic mobile robot, the posture is usually represented by its position (x, y) and orientation $\theta \in [0, 2\pi)$ with respect to X axis, denoted as $p = [x, y, \theta]^T$. The motion is controlled directly by linear velocity v and angular velocity ω or velocities of two driving wheels, which are equivalent to each other. Then, its kinematics is modeled as

$$\begin{cases} \dot{x} = v \cos(\theta), \\ \dot{y} = v \sin(\theta), \\ \dot{\theta} = \omega. \end{cases} \quad (1)$$

Accordingly, the discrete form of (1) is given by

$$\begin{cases} x(t_i^c) = x(t_{i-1}^c) + v(t_{i-1}^c) \cdot \cos(\theta(t_{i-1}^c)) \cdot T, \\ y(t_i^c) = y(t_{i-1}^c) + v(t_{i-1}^c) \cdot \sin(\theta(t_{i-1}^c)) \cdot T, \\ \theta(t_i^c) = \theta(t_{i-1}^c) + \omega(t_{i-1}^c) \cdot T, \end{cases} \quad (2)$$

where T is the motion control period, and t_i^c ($i = 1, 2, \dots$) denotes the control time instant satisfying $t_i^c - t_{i-1}^c = T$. The motion control aims to drive the robot toward its desired posture $p^* = [x^*, y^*, \theta^*]^T$ to achieve predefined tasks by designing the velocities v and ω . Define the instantaneous posture error as $p_e = p^* - p = [x_e, y_e, \theta_e]^T$, and the controller can be represented as

$$\begin{bmatrix} v \\ \omega \end{bmatrix} = \begin{bmatrix} u_v(p_e, \dot{p}_e) \\ u_\omega(p_e, \dot{p}_e) \end{bmatrix}, \quad (3)$$

where u_v and u_ω are designed to control v and ω such that the tracking error $\|p_e\|_2$ goes to zero. Note that (3) represents a general first-order motion control for nonholonomic mobile robots. Many works have been developed with stability guarantees [40]–[42]. They usually require the measurements of \dot{p}^* and are of proportional-derivative-trigonometric type².

Considering the nonlinear characteristic of non-holonomic robots, it is common to introduce a “hand” position $h = [x_h, y_h]^T = [x + d_h \cos \theta, y + d_h \sin \theta]^T$ to simplify the motion control, where d_h is a distance starting from p along the orientation axis. Taking h into (1), one has

$$\begin{bmatrix} \dot{x}_h \\ \dot{y}_h \end{bmatrix} = \begin{bmatrix} \cos \theta & -d_h \sin \theta \\ \sin \theta & d_h \cos \theta \end{bmatrix} \begin{bmatrix} v \\ \omega \end{bmatrix}. \quad (4)$$

By output feedback linearization, the controller for (v, ω) can be designed as [43]

$$\begin{bmatrix} v \\ \omega \end{bmatrix} = \begin{bmatrix} \cos \theta & \sin \theta \\ -\frac{1}{d_h} \sin \theta & \frac{1}{d_h} \cos \theta \end{bmatrix} \begin{bmatrix} u_x(x_e, \dot{x}_e) \\ u_y(y_e, \dot{y}_e) \end{bmatrix}, \quad (5)$$

which gives the following simplified point regulation of the hand position

$$\begin{bmatrix} \dot{x}_h \\ \dot{y}_h \end{bmatrix} = \begin{bmatrix} u_x(x_e, \dot{x}_e) \\ u_y(y_e, \dot{y}_e) \end{bmatrix}, \quad (6)$$

The controller (6) is decoupled and designed in proportional-derivative form to guarantee the stability of h .

There are a few works focusing on directly controlling the applied torque and force for the wheels based on p_e [43],

¹Although learning-based method is commonly said data-driven, the model is generally injective mapping once the training is completed.

²The introduction of the trigonometric function is mainly caused by the decomposition of linear velocity. For example, in [42], the motion controller is designed as $v = v^* \cos \theta^e + k_x x^e$, $\omega = \omega^* + k_\theta \theta^e + v^* y^e \sin \theta^e / \theta^e$.

[44], which is essentially a second-order controller. In this paper, we do not focus on specific motion controller design, but emphasize that the desired posture of the robot can be affected to achieve our attack no matter what motion controller the robot uses.

As for a holonomic mobile robot, the kinematics in two directions is independent and its discrete form is given by

$$\begin{cases} x(t_i^c) = x(t_{i-1}^c) + v_x(t_{i-1}^c) \cdot T, \\ y(t_i^c) = y(t_{i-1}^c) + v_y(t_{i-1}^c) \cdot T, \end{cases} \quad (7)$$

where v_x and v_y are velocities along X and Y axis directions, respectively. Since the motion of a holonomic robot is a direct composition of the motions in two directions, the orientation is usually neglected. Therefore, different from (3), here the motion control is directly formulated as

$$\begin{bmatrix} v_x \\ v_y \end{bmatrix} = \begin{bmatrix} u_x(p_x, \dot{p}_x) \\ u_y(p_y, \dot{p}_y) \end{bmatrix}. \quad (8)$$

The proposed intelligent attack in this paper applies to both kinds of robots. Hereafter, we mainly illustrate our work on non-holonomic robots. It is easy to extend the results to holonomic ones due to the simple motion characteristic, and they will be briefly discussed.

B. Obstacle-avoidance Behavior Modeling

The obstacle-avoidance mechanism is the major interface for a robot to interact with the physical environment, and is universally needed for the robot to work. Let p_{ob} and v_{ob} be the state and velocity of the obstacle, respectively. Considering that avoidance behavior is mainly determined by the relative posture and motion between the robot and the obstacle, we formulate it as the following general function

$$u_{ob} = f(p_{ob} - p, p^* - p, v_{ob}, v), \quad (9)$$

where p^* is the instantaneous desired posture determined by a specific task (e.g., it can represent the target leader posture in formation control). In some algorithm designs, the influence of $(p^* - p)$ is negligible when p_{ob} is very close to p .

Next, we characterize the obstacle-avoidance behavior under (9). Let $\mathcal{A}_d(p)$ be the obstacle detection area of a robot. The obvious characteristic of f is its boundedness regardless of the detailed design, which can be described as

$$\begin{cases} \|f(\cdot)\|_2 = 0, & \text{if } p_{ob} \notin \mathcal{A}_d(p), \\ 0 \leq \|f(\cdot)\|_2 \leq \bar{u}_{ob}, & \text{if } p_{ob} \in \mathcal{A}_d(p), \end{cases} \quad (10)$$

where \bar{u}_{ob} is the output bound. Another salient characteristic is the directionality of the obstacle-avoidance behavior. For ease of expressions, let \mathcal{T}_ϑ be a general notation for a simple curve (trajectory) that divides the X-Y plane into two parts, \mathcal{T}_ϑ^+ and \mathcal{T}_ϑ^- (the subscript ϑ will be replaced when indicating a specific trajectory). Define $I_T(\mathcal{T}_\vartheta, p)$ as the indication function

$$I_T(\mathcal{T}_\vartheta, p) = \begin{cases} 0, & \text{if } p \in \mathcal{T}_\vartheta; \\ +1, & \text{if } p \in \mathcal{T}_\vartheta^+; \\ -1, & \text{if } p \in \mathcal{T}_\vartheta^-. \end{cases} \quad (11)$$

Then, when an obstacle occurs in the detection range at moment k (i.e., $p_{ob} \in \mathcal{A}_d(p(k))$) and $\mathcal{T}_m(p)$ is the instantaneous

tangent line of the robot's motion, the obstacle-avoidance behavior satisfies

$$I_T(\mathcal{T}_m(p(k)), p_{ob}) \cdot I_T(\mathcal{T}_m(p(k)), p(k+1)) < 0, \quad (12)$$

which indicates that the robot will move towards the opposite side of the obstacle taking $\mathcal{T}_m(p(k))$ as a boundary.

There are some notable points about the obstacle-avoidance modeling in some complicated cases.

- Geometric shape. In practice, the obstacle is detected by the sensors as a series of dense points, and the avoidance reaction is based on processing these points by certain computation rules. For example, they can be enclosed by a convex geometric shape that has a simple representation (e.g., a circle) and the robot moves around the central point with a known radius [45].
- Multiple obstacles. When multiple obstacles are involved, the robot will evaluate the influences of the obstacles and obtain their composite impact. In some simple cases, the robot can directly take the nearest obstacle into its avoidance procedures at the moment, which always guarantees a safe avoidance behavior.

The avoidance model (9) covers a majority of algorithms that are based on local detection range and use the obstacle's instantaneous motion state as the input. Considering when the obstacle is moving, some advanced methods are developed to improve the avoidance efficiency by predicting and evaluating the motion of the obstacle [46]–[49]. Nevertheless, these methods usually require some prior knowledge, e.g., the obstacles are assumed to move along deterministic paths [48] or satisfy certain nominal kinematic constraints [49]. Based on the above analysis, we make the following assumption throughout this paper.

Assumption 1. *The obstacle-avoidance detection range of the victim robot is local, and the obstacle-avoidance algorithm it uses can be modeled by (9) and is an injective mapping. Besides, the observations of the attack robot on the victim robot are corrupted with Gaussian noise $\mathcal{N}(0, \sigma^2)$.*

Remark 1. *For the class of moving obstacle avoidance algorithms with prior knowledge acquired, the attack idea and procedure proposed in this paper can still be applied with additional computation costs and higher algorithm complexity, which come from the two aspects. First, the historical positions and velocities of the obstacle itself need to be considered for modeling and learning the mechanism f . Second, the search space during attack implementation should also be increased according to the time horizon used for learning f .*

C. Problem of Interest

Denote the malicious attack robot and the victim robot as R_a and R_v , respectively, and let f represent the obstacle-avoidance mechanism. Our work applies to a basic and representative application scenario where R_v is performing a go-to-goal task and able to detect and avoid obstacles occurring in its surroundings by f . Concretely, R_a aims to fool R_v into a preset trap p_t by disguising as an obstacle, while it can observe (or sense) R_v and has limited moving capability in this process.

Define \mathcal{J} as the observed dataset reflecting f , and the attack is mathematically transformed to solve the following problems.

- Learning f : given \mathcal{J} , find the mapping relation ϕ that embodies f by solving

$$\min_{\phi(\mathcal{J}) \rightarrow f} \|f - \hat{f}\|_2. \quad (13)$$

- Attack strategy design: given \hat{f} , find a group of attack inputs $\mathbf{u}_{a,0:H}$ that drives R_v into p_t by solving

$$\mathbf{P}_0 : \quad \min_{H, \mathbf{u}_{a,0:H}} C_{\vartheta}(\mathbf{u}_{a,0:H}) \quad (14)$$

$$\text{s.t.} \quad \|p_v(H) - p_t\|_2 \leq \delta,$$

where C_{ϑ} is the attack cost (e.g., attack path length or activity period) and $\delta \geq 0$ is a constant that indicates attack termination.

To solve problem (13), the key point is to capture the essential principle about how the mobile robot will adjust its trajectory after an obstacle is detected nearby, and construct a corresponding dataset from observations. For problem (14), it is extremely hard to get an optimal analytic solution due to the implicit form of f . Nevertheless, borrowing ideas from the sampling-based approaches [50], [51], we are able to design efficient algorithms to obtain suboptimal solutions in terms of different attack costs. The whole framework of this paper is shown in Fig. 2.

IV. LEARNING SCHEME FOR OBSTACLE-AVOIDANCE MECHANISM

When R_a encounters an obstacle within its detection area, it will evaluate the obstacle's influence and take corresponding actions, deviating from its desired trajectory. Inspired by this, a learning scheme for the obstacle-avoidance mechanism is proposed. This scheme consists of three parts:

- Pre-sampling. Ideally, the instantaneous motion information of R_v (such as orientation, linear, angular and acceleration velocities) can be obtained based on three consecutive position samplings. This constitutes the cornerstone of the following steps.
- Intentional excitation. With the ability of observing R_v 's motion, R_a intentionally excites R_v by approaching it as a detected obstacle. Then, R_v is steered to generate various obstacle-avoidance behaviors, enriching the observations to learn the underlying mechanism.
- Modeling learning. Based on the collected data of the excitation trials, R_a computes the featured process variables that exhibit the obstacle-avoidance behavior, and regresses the underlying mechanism (9) by learning-based methods (e.g., SVR, RRT).

A. Pre-sampling: Data Acquisition

Recall that the posture p of a mobile robot is updated every control period T , and its trajectory during the period T can be approximated as a straight line. Equipped with advanced sensors, R_a is able to measure its relative displacement with a moving object. Let the sampling period of R_a be $\tilde{T} = NT$, and denote by t_k^s the k -th sampling time satisfying $t_k^s - t_{k-1}^s = \tilde{T}$.

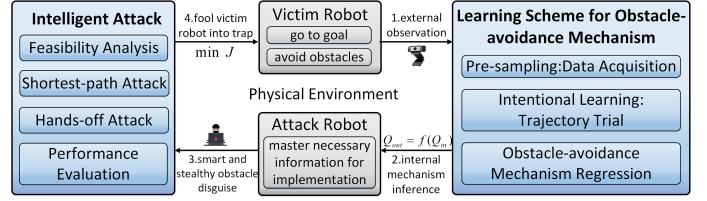


Fig. 2. The architecture of the proposed intelligent physical attack. The primary goal of R_a is to learn the knowledge about the f . Then, with a learned f , efficient attack strategies for different attack requirements are designed to achieve the final purpose.

For simplicity, we use the subscript k to denote the sampling time, e.g., x_k represents the $x(t_k^s)$.

After three consecutive sampling moments, the instantaneous variables of R_v 's motion are estimated by

$$\begin{cases} v_{x,k+1} = \frac{x_{k+1} - x_k}{\tilde{T}}, & v_{y,k+1} = \frac{y_{k+1} - y_k}{\tilde{T}}, \\ v_{k+1} = \sqrt{v_{x,k+1}^2 + v_{y,k+1}^2}, & \theta_{k+1} = \arctan \frac{v_{y,k+1}}{v_{x,k+1}}, \\ a_{k+1} = \frac{v_{k+1} - v_k}{\tilde{T}}, & \omega_{k+1} = \frac{\theta_{k+1} - \theta_k}{\tilde{T}}, \end{cases} \quad (15)$$

where v, w, a represent the linear, angular and accelerated velocities, respectively. Note that R_a should have the latest three groups of observations to calculate (15). For holonomic mobile robots, this process is much easier with higher precision, and v_x, v_y can be directly used. To make a unified statement, let $v_1 = v, v_2 = \omega$ if the robot is non-holonomic or $v_1 = v_x, v_2 = v_y$ if holonomic.

Remark 2. Generally, the motion control period T is very small in practice (e.g., 0.05s or 0.1s), and the sampling period \tilde{T} is determined by the information sensing and processing ability that R_a could afford. Note that the influence of observation noises can be largely weakened if one set a larger sampling period and then calculate an average value in a smaller period (e.g., T). This will not jeopardize the following analysis for the learning and attack procedures.

Note (15) is a noise-free formulation and the real observation of R_a are corrupted with Gaussian noise $\mathcal{N}(0, \sigma^2)$. According to the 3σ -principle [52], for Gaussian distribution with zero expectation value, the variable locates in $[-3\sigma, +3\sigma]$ with probability 0.997, and this interval is basically regarded as the actual range. Therefore, we take 3σ as the maximum error bound of the corresponding measurement in this paper. And the analysis of the measurement noise will be given later.

For R_a , it also needs to discriminate what type R_v is first. This can be done by checking the smoothness of the reaction trajectory, for the velocity direction of the holonomic robot is easy to change suddenly while that of the non-holonomic robot is strictly constrained. Based on (15), R_a can master R_v 's instantaneous motion information of any time. This constitutes the foundation of the following steps.

B. Intentional Excitation: Trajectory Trial

The obstacle detection area of R_v can be generalized to a circular region mostly. If we do not consider obstacles behind

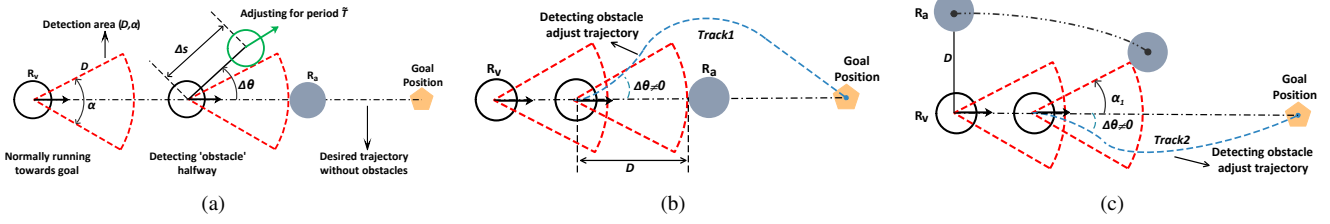


Fig. 3. Illustration of the learning process for R_a. (a) R_v's reaction after detecting R_a as an obstacle. (b) Learning R_v's detection radius D . (c) Learning R_v's detection angle α_1 (α_2 is learned likewise at the other side).

the robot when it moves forward, the detection area is modeled as a sector directly. Then, at this stage, the primary objective of R_a is to infer the radius D and angle range α of the sector, which are together denoted as (D, α) .

When R_a moves close to R_v, R_a makes a record of R_v's relative position, heading and bearing with it. After a period \tilde{T} , R_a does the measurement again. With the two readings, R_a is able to calculate R_v's position variation Δs and heading variation $\Delta\theta$ after \tilde{T} , as shown in Fig. 3(a). During time slot $[t_k^s, t_{k+1}^s]$, we have

$$\begin{cases} \Delta s(k) = \sqrt{(\Delta x_{k,k+1})^2 + (\Delta y_{k,k+1})^2}, \\ \Delta\theta(k) = \arctan \frac{\Delta y_{k,k+1}}{\Delta x_{k,k+1}}, \end{cases} \quad (16)$$

where $\Delta x_{k,k+1} = x(t_k^s + \tilde{T}) - x(t_k^s)$ and $\Delta y_{k,k+1} = y(t_k^s + \tilde{T}) - y(t_k^s)$. Let p_g represent the goal position of R_v. In normal situations, R_v goes straight forward to p_g , i.e., $\Delta\theta = 0$. Therefore, R_a is detected as an obstacle within (D, α) by R_v if $\Delta\theta \neq 0$. Meanwhile, after the orientation of R_a becomes stable, R_a also records the trajectories of R_v moving straightforward to p_g , as shown in Fig. 3(b) and 3(c).

It is remarkable that when the mission area is obstacle-free, moving straight to the goal position is the most efficient way. There are also cases where the robot is specified to go to the goal in a smooth curve, and we can utilize classic polynomial fitting technique to approximate the trajectory [53]. Let n_p be the polynomial order, $\tilde{x} = [x^{n_p}, x^{n_p-1}, \dots, x^0]^T$ and $\mathbf{P} \in \mathbb{R}^{n_p+1}$ be the coefficient vector associated with \tilde{x} . A point in the trajectory is modeled as

$$y = \mathbf{P}^T \tilde{x} + \eta, \quad (17)$$

where η is i.i.d. Gaussian noise satisfying $N(0, \sigma^2)$. Then, the problem is transformed to find the best \mathbf{P} from groups of linear equations (17), where the solving procedures are the same as that of a straight line ($n_t = 1$ in this case). Therefore, we mainly focus on the latter case for simplicity.

Repeatedly, suppose there are n_z groups of trajectories recorded, and the observed points associated with l -th trajectory satisfy

$$\mathcal{T}_r^{(l)}: y_{lj} = \mathbf{P}_l^T \tilde{x}_{lj} + \eta_{lj}, \quad j = 1, 2, \dots, n_t, \quad (18)$$

where n_t is the number of recorded points in this trajectory. Let $d_T(\mathcal{T}_\vartheta, p)$ be the minimal distance from a position p to \mathcal{T}_ϑ , and we obtain the following result.

Theorem 1 (Estimate the goal position). *Given n_t observed points in $\mathcal{T}_r^{(l)}$, if $n_t \rightarrow \infty$, the estimated $\mathcal{T}_r^{(l)}$ will pass through p_g , satisfying*

$$\lim_{n_t \rightarrow \infty} d_T(\mathcal{T}_r^{(l)}, p_g) = 0. \quad (19)$$

Given trajectories $\{\mathcal{T}_r^{(l)}, l = 1, \dots, n_z\}$ and let $\hat{p}_g(n_z)$ be the corresponding least square estimator of the goal position p_g . If $n_z \rightarrow \infty$, p_g is accurately estimated, i.e.,

$$\lim_{n_z \rightarrow \infty} \|\hat{p}_g(n_z) - p_g\|_2 = 0. \quad (20)$$

Proof. The proof is provided in Appendix A. \square

Remark 3. *Theorem 1 illustrates how the accuracy is influenced by the recorded trajectories, where n_t determines how close p_g is to a recorded trajectory while n_z determines how close p_g is to \hat{p}_g . Specifically, according to Chebyshev inequality (as shown in the proof of Theorem 1), the estimation errors of a single trajectory $\mathcal{T}_r^{(l)}$ and \hat{p}_g go to zero at the rate of $O(\frac{1}{n_t})^3$ and $O(\frac{1}{n_z})$, respectively.*

If there are other obstacles occurring in R_v's detection area, an efficient way for R_v is adding up the impacts of the obstacles and using the composite impact as the instantaneous recorded input. Meanwhile, the attack process of R_a will simultaneously take R_v and other obstacles into account. Considering the possibility that R_a's sensor view may be blocked by other obstacles, R_a can be equipped with advanced onboard sensors at an appropriate height, e.g., deploying an omnidirectional camera on the top of R_a. Also, R_a can actively move to other positions such that R_v is observed, as in the intentional learning stage.

C. Model learning: SVR-based method

When (D, α) of R_v is obtained, R_a is controlled to excite R_v by blocking in (D, α) . In this step, R_a also records its relative distance d_{va} and bearing φ_r with R_v, and R_v's heading deviation θ' with p_g . Once R_a is detected by R_v, R_a stores two groups of data during the next period \tilde{T} . The data groups are defined as

$$\begin{cases} Q_{in}(k) = [\theta'(k), v_1(k), v_2(k), a(k), d_{va}(k), \varphi_r(k)]^T, \\ Q_{out}(k) = [\Delta s(k), \Delta\theta(k)]^T. \end{cases} \quad (21)$$

³For two real-valued functions f_1 and f_2 , $f_1(x) = O(f_2(x))$ as $x \rightarrow x_0$ means $\lim_{x \rightarrow x_0} |f_1(x)/f_2(x)| < \infty$.

Algorithm 1 Excitation-based Obstacle-avoidance Learning

Input: Posture regulating variables $\Delta d, \Delta\alpha$, constant k_{\max} , $\mathcal{J} = \emptyset$
Output: Detection area (D, α) , p_g and f

- 1: **Initialize:** R_a moves to remote posture p_a such that R_a is directly ahead of R_v and $\varphi_r = 0$
- 2: **while** $\Delta\theta = 0$ **do**
- 3: R_a moves towards R_v such that $d(p_a, p_v) = d(p_a, p_v) - \Delta d$, and calculate $\Delta\theta$ by (16)
- 4: **end while**
- 5: Record D , and the following trajectory as $\mathcal{T}_r^{(1)}$. Then reset R_a such that $d(p_a, p_v) = D$ and $\varphi_r = +90^\circ$
- 6: **while** $\Delta\theta = 0$ **do**
- 7: R_a moves towards R_v such that $\varphi_r = \varphi_r - \Delta\alpha$, and calculate $\Delta\theta$ by (16)
- 8: **end while**
- 9: Record $\alpha_1 = \varphi_r$, and following trajectory $\mathcal{T}_r^{(2)}$. Reset R_a such that $d(p_a, p_v) = D$ and $\varphi_r = -90^\circ$. Then R_a does the same process again to obtain a new α_2 and $\mathcal{T}_r^{(3)}$
- 10: $\alpha = [\alpha_2, \alpha_1]$, and use the trajectories to compute p_g by least square method
- 11: Reset R_a such that R_a is outside (p_v, D, α)
- 12: **for** $k \leftarrow 1$ **to** k_{\max} **do**
- 13: R_a randomly moves to $p_a \in (p_v, D, \alpha)$, and compute $Q_{in} = [\theta', v_1, v_2, a, d_{va}, \varphi_r]$ at t_k^s ;
- 14: Wait for a time slot \tilde{T} , compute $Q_{out} = [\Delta s, \Delta\theta]$ at t_{k+1}^s , and $\mathcal{J} = \mathcal{J} \cup \{Q_{in}, Q_{out}\}$;
- 15: **end for**
- 16: Use \mathcal{J} and learning-based method (e.g., SVR) to regress f
- 17: **Return** (D, α) , p_g and f .

Accordingly, the obstacle-avoidance knowledge dataset \mathcal{J} is constructed by

$$\mathcal{J} = \left\{ \bigcup_{k \in \mathcal{F}} \{Q_{in}(k), Q_{out}(k)\} \right\}, \quad (22)$$

where $\mathcal{F} = \{k \in \mathbb{N}^+ : d_{va}(k) \leq D, \varphi_r(k) \in \alpha\}$.

Based on above analysis, the whole steps of intentional learning is designed as Algorithm 1, by which R_a learns the obstacle-detection area (p_v, D, α) and goal position p_g [Line 2-10], and regresses obstacle-avoidance mechanism f of R_v [Line 11-16], respectively. The complexity of Algorithm 1 is simply determined by the number of the required observations, where R_a just moves to obtain the required independent observations and does not involve other specific computation procedures. Taking p_g as an example, two independent groups of observations ($n_z = 2$) on two non-parallel trajectories ($n_t = 2$) towards p_g are sufficient to obtain an accurate \hat{p}_g in the ideal noise-free situation. As Remark 3 indicates that the estimation error will decay to zero at a rate of $\mathcal{O}(\frac{1}{n_t})$ in noisy situations, setting $n_z = 3$ and $n_t = 30$ would be sufficient for our purpose, which is also verified in simulations. If the position and motion parameter settings change, one only needs to sample more observations to ensure a reliable \hat{p}_g .

SVR method has good performance on non-linear regression and strong generalization ability when the amount of data isn't vast. It is insensitive to the models of the objects and has a certain tolerance for data noises, due to the ϵ -error tube design [54]. Thus it is adopted in this paper to learn the obstacle-avoidance mechanism using the collected data, which can be

formulated as solving the following problem

$$\begin{aligned} \min_{\omega, \beta, \tilde{\xi}_k^-, \tilde{\xi}_k^+} & \frac{1}{2} \|w\|^2 + C \sum_{k=1}^{|\mathcal{J}|} (\tilde{\xi}_k^- + \tilde{\xi}_k^+) \\ \text{s.t.} & f(Q_{in}(k)) - Q_{out}(k) \leq \epsilon + \tilde{\xi}_k^-, \\ & Q_{out}(k) - f(Q_{in}(k)) \leq \epsilon + \tilde{\xi}_k^+, \\ & f(Q_{in}(k)) = w^\top \psi(Q_{in}(k)) + \beta, \\ & \tilde{\xi}_k^- \geq 0, \tilde{\xi}_k^+ \geq 0, k = 1, 2, \dots, |\mathcal{J}|, \end{aligned} \quad (23)$$

where $C > 0$ is the regularization parameter for the ϵ -sensitive loss function, $\tilde{\xi}_k^-$ and $\tilde{\xi}_k^+$ are two slack variables, $\psi(Q_{in}(k))$ represents the mapping feature vector of $Q_{in}(k)$ and can be dealt by the commonly used kernel tricks. The obtained ω , β and the selected kernels together constitute the final learned obstacle-avoidance mechanism \hat{f} . More details about the solving process of the SVR can be found in [54].

It is worth noting that SVR method utilizes a ϵ -tube as a regularization technique to improve the model robustness, which acquires certain tolerance for the observation noises. Also, since the observation noise of Q_{out} accumulates during the observation period \tilde{T} , the learning method will achieve the ideal performance if $\tilde{T} \rightarrow T$. In addition, although the learned \hat{f} is a mapping from Q_{in} to Q_{out} , the model is not necessarily a surjective or injective mapping. In other words, \hat{f} cannot be inversely used to obtain the input given outputs in most cases.

The discrepancy of regression for different obstacle-avoidance algorithms embodies in the internal structure and parameters of the regression model. With the obstacle-avoidance mechanism learned by R_a , it fills the gap between the strong assumption (where the attacker has known the information of the target system from the very beginning), and the real implementation (where the attacker needs to acquire the necessary information first).

V. ATTACK STRATEGY DESIGN AND ANALYSIS

In this section, we propose the shortest-path attack and hands-off attack strategies to achieve the final purpose. First, the feasibility of the attack strategies is analyzed. Then, we present the detailed design of the strategies. Finally, the attack performance bounds and conditions are derived to illustrate the effectiveness of our proposed methods.

A. Attack Idea and Feasibility

In this part, we demonstrate the ideas of the proposed attack strategies and analyze their feasibility.

Since path distance is a commonly-used optimization objective in robot path planning [55], we first propose the shortest-path attack strategy for R_a , which aims to drive R_v into the preset trap with minimal path cost. Note that R_a is in a consistently active state during the shortest-path attack process, which is not desirable in some cases. For example, long-time obstacle occurrence nearby may cause an anomaly alarm of R_v and even make R_v alter the control strategy. To alleviate these effects and make R_a stealthier, we further propose hands-off attack strategy. ‘‘Hands-off’’ means the control effort over the plant can be maintained exactly at zero over a time interval

and aims to obtain the sparsest control or the minimal active interference with the plant [56], [57].

The feasibility of our proposed strategies lies in two aspects. First, the proposed attack is launched from the physical world by making R_a disguise as an obstacle in front of R_v , and the presence of R_a is taken into consideration by f , making R_v unable to ignore the influence. Second, the learning scheme proposed in the last section enables R_a to acquire the obstacle-avoidance knowledge of R_v , providing reliable support for a more efficient and intelligent strategy design. Specifically, the major issue is to address the coupled dynamics of R_a and R_v , and the nonanalytic property brought by the learned \hat{f} .

Based on the learned knowledge about f , the obstacle detection area of R_v is formulated as

$$\mathcal{A}_d(p_v) = \{p : \|p - p_v\|_2 < D, \alpha_1 \leq \langle \overrightarrow{pp_v}, \mathcal{T}_m(p_v) \rangle \leq \alpha_2\}, \quad (24)$$

where $\langle \overrightarrow{pp_v}, \mathcal{T}_m(p_v) \rangle$ is the angle between the vector $\overrightarrow{pp_v}$ and the motion orientation $\mathcal{T}_m(p_v)$.

Regardless of the robot type, the motion updates of R_v and R_a are represented as

$$p_v(k+1) = h_v(p_v(k), u_v(k)), \quad (25)$$

$$p_a(k+1) = h_a(p_a(k), u_a(k)), \quad (26)$$

where $u_v(k)$ is the velocity control input of R_v and $u_a(k)$ is attack input of R_a . With learned \hat{f} , the velocity input and position of R_v are respectively predicted by

$$\hat{u}_v(k) = \hat{f}(p_a(k), p_v(k), u_v(k-1)), \quad (27)$$

$$\hat{p}_v(k+1) = h_v(p_v(k), \hat{u}_v(k)). \quad (28)$$

B. Shortest-path and Hands-off Attack Algorithms

First, we introduce the shortest-path attack. Since the obstacle-avoidance process under f is a dynamic trade-off between avoiding the obstacle and going to goal, there exists a certain moment, before which the obstacle-avoidance part plays a dominant role and after which the go-to-goal does. The key point of the shortest-path attack strategy is to impose a consistent impact on the former one as large as possible, such that R_v is generally dominated by R_a into p_t .

Denote the initial attack position as p_{a_0} , and the attack path is the trajectory of R_v that starts from p_{a_0} and ends at p_t . Then, to obtain the minimal attack path length, the original attack design problem \mathbf{P}_0 is rewritten as the following problem.

$$\mathbf{P}_1 : \min_{H, \mathbf{u}_{a,0:H}} C_s(\mathbf{u}_{a,0:H}) = \sum_{k=0}^H \|\hat{p}_v(k+1) - p_v(k)\|_2, \quad (29a)$$

$$\text{s.t.} \quad \|u_a(k)\|_2 \leq \mu, \quad (29b)$$

$$\|p_v(H) - p_t\|_2 \leq \delta, \quad (29c)$$

$$\eta \leq \|p_a(k) - p_v(k)\|_2, \quad (29d)$$

$$p_a(k) \in \mathcal{A}_d(p_v(k)), \quad (29e)$$

$$(25), (26), (27), \text{ and } (28),$$

where μ , δ , and η are all positive constants, and the constraints hold for all $k \in \{0, \dots, H\}$. In (29), the first constraint (29b) demonstrates the boundness of the attack inputs, and the second constraint (29c) guarantees that R_v is close enough

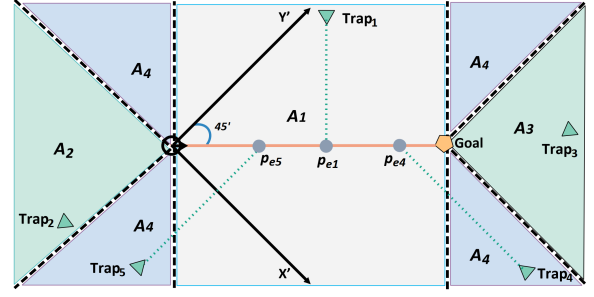


Fig. 4. Illustration of the choice for entry point. To save the page space, we rotate the $X'-Y'$ coordinate frame 45° clockwise. The $X'-Y'$ plane is divided into four parts using dash lines and different colors: the gray area between two vertical dash lines is \mathcal{A}_1 , the green area between the two left clinodiagonal dashed lines is \mathcal{A}_2 , the green area between the two right clinodiagonal dashed lines is \mathcal{A}_3 , and the left blue region is \mathcal{A}_4 . The entry point of $Trap_1$, $Trap_4$ and $Trap_5$ is p_{e1} , p_{e4} and p_{e5} , respectively.

to p_t when the attack stops. The η in (29d) is designed to keep a safe distance between R_a and R_v to avoid possible collision at next move, and (29e) makes sure that R_a is always in the detection area during the attack. The last four constraints capture the state dynamics of R_a and R_v .

Ideally, the shortest attack path \mathcal{T}_a is directly obtained by connecting p_{a_0} and p_t . However, \mathcal{T}_a is almost impossible to be the real optimal trajectory, because the mechanical structure and control dynamics constraints of R_v will not allow the sudden turn point and the trajectory rigidity in \mathcal{T}_a . Even so, we are able to take \mathcal{T}_a as evaluation criteria: the closer the obtained attack trajectory is with \mathcal{T}_a , the better the attack strategy is. Then comes an interesting problem: how to choose the best p_{a_0} to begin attacking, which we call entry point.

Denote by \mathcal{T}_g the trajectory from the initial position $p_v(0)$ to p_g without being attacked. Then, the definition of the entry point is given as follows.

Definition 1. (Entry point) *Given a configuration of $p_v(0)$, p_g , and p_t , rebuild a coordinate frame $X'-Y'$ where the Y' positive axis is at a angle of 45° to \mathcal{T}_g . Divide the $X'-Y'$ plane into four parts using dash line (as shown in Fig. 4). Then, the entry point p_e is defined as follows*

- i) If $p_t \in \mathcal{A}_1$, p_e is the vertical projection of p_t onto \mathcal{T}_g , i.e.,

$$p_e = \arg \min_{p'} \|p' - p_t\|_2^2, \quad (30)$$

where $p' \in \{p : I_T(\mathcal{T}_g, p) = 0\}$.

- ii) If $p_t \in \mathcal{A}_2$, there is no exact position of p_e . Under given constraints, the earlier to attack, the better.
- iii) If $p_t \in \mathcal{A}_3$, there is no exact position of p_e . Under given constraints, the later to attack, the better.
- iv) If $p_t \in \mathcal{A}_4$, p_e is the projection of p_t along X' or Y' direction onto \mathcal{T}_g .

Given a preset small threshold $r_d > 0$ (e.g., it can be set as the smallest position deviation between two observation moments), if $\|p_v(k) - p_e\|_2 \leq r_d$ holds for the first time during R_v 's movement towards p_g , then set $a_s = k$. Next, R_a begins

Algorithm 2 Shortest-path Attack Strategy

Input: \hat{f} , the iteration limit k_{\max} , and tolerant bound δ .
Output: Terminal horizon H , and attack input vector $\mathbf{u}_{a,0:H}$;
 1: Initialize $p_v(0)$, p_g , p_t , and set the attack signal $a_s = 0$;
 2: Compute entry point p_e by (30);
 3: Randomly select a $p_a(0)$ such that $\|p_a(0) - p_e\| \leq r_d$;
 4: R_v starts to run towards p_g , $\mathcal{A}_a^f = \emptyset$;
 5: **for** $k \leftarrow 1$ **to** k_{\max} **do**
 6: **if** $a_s = 0$ and $\|p_v - p_e\| \leq r_d$ **then**
 7: R_a moves into the pre-attack position, $a_s = k$;
 8: **else**
 9: R_a stays still;
 10: **end if**
 11: **if** $a_s \geq 1$ **then**
 12: Uniformly sample a subset $\mathcal{A}_a^{\text{rand}} \subseteq \mathcal{A}_d(p_v(k))$;
 13: **for** $p_a(k+1) \in \mathcal{A}_a^{\text{rand}}$ **do**
 14: Compute $\hat{p}_v(k+1)$ by (28);
 15: $\hat{d}_{vt}(k+1) = \|\hat{p}_v(k+1) - p_t\|_2$, $d_{vt}(k) = \|p_v(k) - p_t\|_2$;
 16: **if** $\hat{d}_{vt}(k+1) \leq d_{vt}(k)$ and $p_a(k+1) \in \mathcal{A}_d(p_v(k))$ **then**
 17: Update $\mathcal{A}_a^f = \mathcal{A}_a^f \cup \{p_a(k+1)\}$;
 18: **end if**
 19: **end for**
 20: $k' = k - a_s$, $u_a(k') = \arg \min_{u_a} \{\|\hat{p}_v(k+1) - p_t\|_2 : p_a(k+1) \in \mathcal{A}_a^f, (29b) \text{ and } (29d) \text{ hold}\}$;
 21: **end if**
 22: **if** $\|p_v(k) - p_t\|_2 < \delta$ **then**
 23: **break**;
 24: **end if**
 25: **end for**
 26: $H = k'$, and construct attack input vector $\mathbf{u}_{a,0:H}$;

attacking by moving to its initial attack position $p_a(a_s + 1)$, which satisfies

$$\begin{cases} p_a(a_s + 1) \in \mathcal{A}_d(p_v(a_s)), \\ I_T(\mathcal{T}_g, p_a(a_s + 1)) \cdot I_T(\mathcal{T}_g, p_t) < 0. \end{cases} \quad (31)$$

Note the second condition in (31) requires the initial attack position and p_t are in opposite positions of \mathcal{T}_g .

Since the intentional learning and attack process are separated (i.e., there is no direct feedback between the two parts), and due to the black-box characteristic of the learned model, obtaining a global analytical solution for the problem is intractable. Therefore, we propose a sampling-based approach and find sub-optimal solutions quickly. The complete process is summarized in Algorithm 2.

Algorithm 2 is composed of three parts: i) before R_v comes near to p_e (determined by the distance threshold $r_d > 0$), R_a needs to wait for the best attack time [Line 6-10]; ii) after R_a begins its attack, every iteration is based on sampling to explore the motion space of both R_a and R_v and select a best attack input from a feasible attack set $\mathcal{A}_a^{\text{rand}}$ [Line 11-21]; iii) when R_v is close enough from p_t (determined by the distance threshold $\delta > 0$), R_a stops and we call the attack is successful [Line 22-24]. Note that the complexity of Algorithm 2 is determined by multiple factors, including the moving offset of R_v , the distance between p_e and p_t , and the granularity of $\mathcal{A}_a^{\text{rand}}$, making it hard to be explicitly characterized. Specially, if R_a can make R_v directly move towards the trap with constant offset L and by referring to the complexity analysis of gradient-descent algorithm, the complexity of Algorithm 2

Algorithm 3 Hands-off Attack Strategy

Input: k_{\max} , \hat{f} , δ (as in Algorithm 2), and preset constant γ ;
Output: H and $\mathbf{u}_{a,0:H}$;
 1: **do** [Line 1-4] of Algorithm 2;
 2: **for** $k \leftarrow 1$ **to** k_{\max} **do**
 3: $d_{vt}(k) = \|p_v(k) - p_t\|_2$, $k' = k - a_s$;
 4: **do** [Line 6-10] of Algorithm 2;
 5: **if** $a_s \geq 1$ and $d_{vt}(k) > \gamma d_{te}$ **then**
 6: **if** $d_{vt}(k) \leq d_{vt}(k-1)$ and (32b), (32d) hold **then**
 7: R_a stays inactive, i.e., $u_a(k') = 0$;
 8: **else**
 9: **do** [Line 12-20] of Algorithm 2 and obtain $u_a(k - a_s)$;
 10: **end if**
 11: **else if** $a_s \geq 1$ and $d_{vt}(k) \leq \gamma d_{te}$ **then**
 12: **if** $d_T(\mathcal{T}_m(p_v(k)), p_t) < \delta$ and (32b), (32d) hold **then**
 13: R_a stays inactive, i.e., $u_a(k') = 0$;
 14: **else**
 15: **do** [Line 12-20] of Algorithm 2 and obtain $u_a(k')$;
 16: **end if**
 17: **end if**
 18: **do** [Line 22-24] of Algorithm 2;
 19: **end for**
 20: $H = k'$, and construct attack input vector $\mathbf{u}_{a,0:H}$;

can be characterized by $\mathcal{O}\left(\frac{\|p_e - p_t\|_2^2}{\delta L}\right)$ (see Chapter 8.3 in [58] for more proof details). This complexity can be regarded as the ideal case where the obstacle-avoidance mechanism is perfectly learned. Despite the intractable complexity analysis for general cases, we can characterize the more concerned performance bounds, which will be provided in Section V-D.

Based on the formulation in the shortest-path attack, we further propose the hands-off attack, which leverages inertia nature that the obstacle-avoidance of R_v is not a one-time effort (i.e., it takes certain time to circumvent the obstacle and adjust to its goal position). Therefore, R_a does not need to move consistently. In this scenario, R_a is at a hands-off state if it stays still at one moment during the attack. To obtain the minimal attack activity period, \mathbf{P}_0 is rewritten as the following hands-off attack design problem.

$$\mathbf{P}_2 : \quad \min_{H, \mathbf{u}_{a,0:H}} C_h(\mathbf{u}_{a,0:H}) = \|\mathbf{u}_{a,0:H}\|_0 \quad (32a)$$

$$\text{s.t.} \quad \|u_a(t)\|_2 \leq \mu, \quad (32b)$$

$$\|p_v(H) - p_t\|_2 \leq \delta, \quad (32c)$$

$$\eta_1 \leq \|p_a(t) - p_v(t)\|_2 \leq \eta_2, \quad (32d)$$

(25), (26), (27), and (28),

where the constraints hold $\forall t \in \{0, \dots, H\}$. In (32), different from (29d) and (29e), (32d) can be seen as their relaxation such that R_a does not have to be in the obstacle detection area all the time. Other constraints are the same as that in \mathbf{P}_1 .

The algorithm design of solving \mathbf{P}_2 is summarized in Algorithm 3. Note that R_a cannot stay inactive all the time, thus the major difference from the shortest-path attack here is to maximize the silent period between two consecutive attacks. To tackle this issue, we introduce a criteria based on $d_T(\mathcal{T}_m(p_v), p_t)$ and $d_{vt}(k) = d(p_v(k), p_t)$. Then, Algorithm 3 can be interpreted as four parts: i) R_a waits for the best attack time first [Line 4], which is similar to Algorithm 2; ii) When $d_{vt}(k)$ is large after the attack begins, R_a uses the change of $d_{vt}(k)$ to determine whether to stay still or move [Line 6-10].

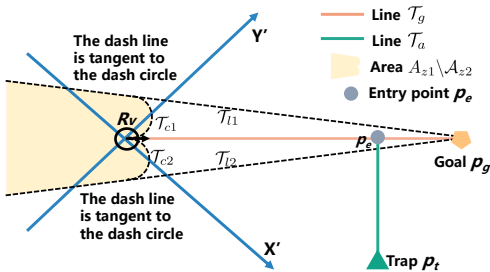


Fig. 5. Illustration of the condition of successful attack.

If it needs to make an attack, the attack inputs are sampled from the motion space of both R_a and R_v and to explore the best one from the feasible attack set; iii) When $d_{vt}(k)$ becomes small, R_a alters to a new attack decision criteria, by which R_a can stay still if $d_T(\mathcal{T}_m(p_v), p_t)$ does not grow larger and the constraints are satisfied [Line 12-16]; iv) Finally, the same stopping criteria as that in Algorithm 2 is adopted [Line 18]. Since Algorithm 3 also enjoys the descent-wise nature, it shares the same complexity scale as Algorithm 2.

C. Attack Conditions and Algorithm Convergence

Next, we give the conditions to successfully realize the attack by the proposed algorithms, and analyze the convergence.

To intuitively describe the trap setting, we mainly use geometric expressions combined with graph illustration. Given p_{v0} and p_g , divide the 2-D plane into the X' - Y' coordinate frame defined in Definition 1. First, draw the two circumcircles with radius r_{\min} , \mathcal{T}_{c1} and \mathcal{T}_{c2} , tangent to \mathcal{T}_g at p_{v0} , respectively. Then, draw the two tangent lines \mathcal{T}_{l1} for \mathcal{T}_{c1} , and \mathcal{T}_{l2} for \mathcal{T}_{c2} , going through p_g . In the X' - Y' coordinate frame, with deterministic p_{v0} , p_g and r_{\min} , the expressions of \mathcal{T}_{c1} , \mathcal{T}_{c2} , \mathcal{T}_{l1} and \mathcal{T}_{l2} are explicitly determined, and are represented as

$$\mathcal{T}_{c1} = \{p : \|p - p_{c1}\|_2^2 - r_{\min}^2 = 0\}, \quad (33)$$

$$\mathcal{T}_{c2} = \{p : \|p - p_{c2}\|_2^2 - r_{\min}^2 = 0\}, \quad (34)$$

$$\mathcal{T}_{l1} = \{p = (x, y)^T : y - a_1x - b_1 = 0\}, \quad (35)$$

$$\mathcal{T}_{l2} = \{p = (x, y)^T : y - a_2x - b_2 = 0\}, \quad (36)$$

where p_{c1} and p_{c2} are the centers of \mathcal{T}_{c1} and \mathcal{T}_{c2} , and $\{a_1, b_1\}$ and $\{a_2, b_2\}$ are the slope-intercept terms of \mathcal{T}_{l1} and \mathcal{T}_{l2} , satisfying $a_1, a_2 > 0, b_1 > 0$ and $b_2 < 0$. Accordingly, we have

$$I_T(\mathcal{T}_{ci}, p) = \text{sign}(\|p - p_{ci}\|_2^2 - r_{\min}^2), \quad (37)$$

$$I_T(\mathcal{T}_{li}, p) = \text{sign}(y - a_i x - b_i), \quad (38)$$

where $i = 1, 2$ and sign is the indication function. Next, we introduce an auxiliary area variable, given by

$$\mathcal{A}_{z1} = \{p : I_T(\mathcal{T}_{l1}, p) \leq 0, I_T(\mathcal{T}_{l2}, p) \geq 0, x \leq x^g, y \leq y^g\}, \quad (39)$$

$$\mathcal{A}_{z2} = \{p : I_T(\mathcal{T}_{c1}, p) \geq 0, I_T(\mathcal{T}_{c2}, p) \geq 0, I_T(\mathcal{T}_{l1}, p) \leq 0, I_T(\mathcal{T}_{l2}, p) \geq 0, \|p - p_g\|_2 \leq \|p_{v0} - p_g\|_2\}. \quad (40)$$

Apparently, as shown in Fig. 5, $\mathcal{A}_{z2} \subseteq \mathcal{A}_{z1}$. Based on these notations, we first obtain the following theorem to demonstrate the convergence of Algorithm 2.

Theorem 2 (Convergence condition of Algorithm 2). *If the trap position $p_t \notin \mathcal{A}_{z1} \setminus \mathcal{A}_{z2}$, then R_a can always drive R_v into p_t by Algorithm 2, i.e.,*

$$\lim_{k \rightarrow \infty} \|p_v(k) - p_t\|_2 = 0. \quad (41)$$

Proof. The proof is provided in Appendix B. \square

Theorem 2 presents the criterion to set p_t . In fact, as Fig. 5 shows, it also demonstrates how the initial configuration of R_a , R_v , the goal and the trap will affect the final attack result. As long as the initial configurations meet the above conditions, the success of Algorithm 2 by utilizing the obstacle-avoidance characteristic of R_v is guaranteed, which will be also verified with various cases in Section VI and VII. There are two points that need to be noted. First, although the given condition is only sufficient to achieve the driving-to-trap attack, it covers quite a large area for most trap settings. To further relax the condition, the key is to explore more advanced strategy design based on more agile moving ability of R_a . Second, as indicated in the Appendix B, the obstacle-avoidance characteristic corresponds to a descent property and Algorithm 2 can be regarded as a descent search algorithm to solve

$$\min_{p_v} F(p_v) = \|p_t - p_v\|_2^2, \quad (42)$$

which is convex about p_v and has only one minima. Note that Algorithm 2 shares similar form with the conventional gradient-descent method and thus effectively solves the problem. The main difference in Algorithm 2 is that the search direction is not a fixed form at each iteration (e.g., not necessarily the negative gradient of $F(p_v)$). By evaluating the most appropriate move from the sampled feasible position set, the algorithm effectively avoids the oscillation issues.

As for the hands-off attack, Algorithm 3 also works as a descent search like Algorithm 2, except that the attack robot is not always active. However, we note that during an inactive period $[k_1, k_2]$ for the attacker, the positions of the victim satisfy $\|p_v(k_2) - p_t\|_2 < \|p_v(k_1) - p_t\|_2$, illustrating that the victim still takes a descent path to the trap. Hence, the victim's movement during this period is equivalent to a special single step, and the convergence of Algorithm 3 is still guaranteed as Algorithm 2.

D. Attack Performance Analysis

In this part, we analyze the attack performance of Algorithms 2 and 3 from the perspective of the path length and activity period, respectively. First, denote by C_s^* the optimal cost of \mathbf{P}_1 , and we have the following result.

Theorem 3 (Existence of ε -approximated solutions). *The optimal cost can be approximated with arbitrary precision, i.e., $\forall \varepsilon > 0$, there exists a $\mathbf{u}_{a,0:H}$ such that $|C_s(\mathbf{u}_{a,0:H}) - C_s^*| \leq \varepsilon$.*

Proof. The proof is provided in Appendix C. \square

Theorem 3 demonstrates the existence of ε -approximated solutions for the optimal cost of \mathbf{P}_1 . To further investigate how good the solution by Algorithm 2 is, we introduce a

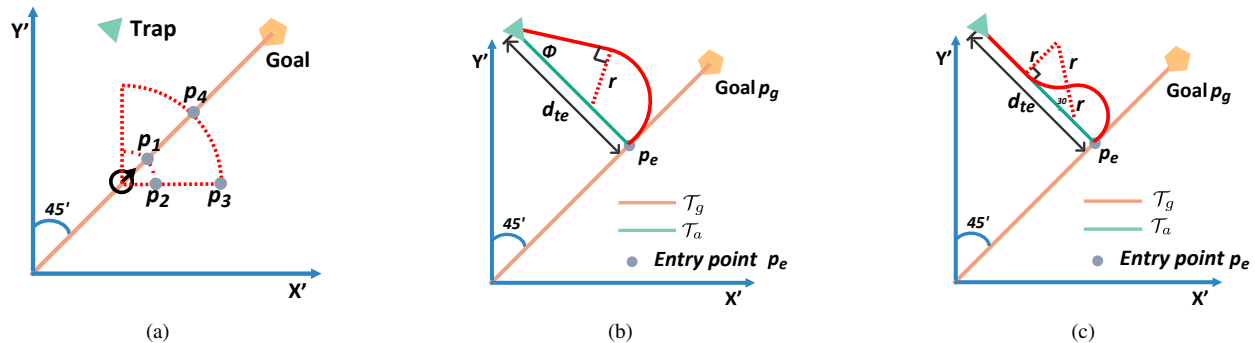


Fig. 6. Shortest-path attack against non-holonomic robot. (a) Illustrations of four special attack positions p_i , $i = 1, 2, 3, 4$. (b) Attack pattern1: a circular arc plus a line segment. (c) Attack pattern2: two circular arcs plus a line segment.

two-tuple (ω, r) to illustrate the visual effect that how a non-holonomic robot avoids an obstacle⁴. As shown in Fig. 6(a), supposing the trap is at the left side of R_v , we denote four extreme positions $\{p_1, p_2, p_3, p_4\}$ where R_a could make an effective attack, along with corresponding output denoted as $\{(\omega_i, r_i), i = 1, \dots, 4\}$. In terms of the reaction radius r_i , p_1 is the most threatening position for R_a while p_3 the least threatening, as $r_1 < r_2 < r_4 < r_3$. Let $r_{\max} = \max\{r_i\}$, $r_{\min} = \min\{r_i\}$, $d_{te} = \|p_t - p_e\|_2$, and denote l_{path} as the trajectory length of R_v under attack. Then, we present the following theorem that gives the performance bounds of Algorithm 2.

Theorem 4 (Performance bounds of Algorithm 2). *Let \bar{C}_s be the cost obtained by Algorithm 2. When $p_e \in \mathcal{A}_1$ and $d_{te} > 2 \cdot r_{\min}$, we have*

$$(\pi/2 + \xi - \cos \xi)r_{\min} + d_{te}(\cos \xi - 1) \leq \bar{C}_s - C_s^* \leq \left(\frac{7}{6}\pi - 1 - \sqrt{3}\right)r_{\max}, \quad (43)$$

where $\xi = \arcsin\left(\frac{r_{\min}}{d_{te} - r_{\min}}\right)$.

Proof. The proof is provided in Appendix D. \square

With the feasibility of the attack guaranteed, Theorem 4 indicates in most situations⁵ how close the solution obtained by Algorithm 2 is to ideal trajectory, and how the worst solution could be, which is extremely hard to actually meet.

Concerning the hands-off attack, the existence of the optimal solution of \mathbf{P}_2 is similar with \mathbf{P}_1 and guaranteed. The proof resembles that of Theorem 3 and is omitted here. Then, the attack performance of Algorithm 3 is presented in the following theorem.

Theorem 5 (Performance bounds of Algorithm 3). *Let H_1 and H_2 denote the attack horizon obtained by Algorithm 2 and 3, respectively, then we have*

$$H_2 \leq 2H_1, \quad (44)$$

and the active attack period by Algorithm 3 satisfies

$$C_h(\mathbf{u}_{a,0;H_2})/H_2 \leq 0.5. \quad (45)$$

⁴For a non-holonomic robot, the output (v, ω) under f also determines the curvature radius r as $v = \omega r$, and (ω, r) is more intuitive to describe the instantaneous obstacle-avoidance behavior.

⁵There is no need to consider $p_t \in \mathcal{A}_1$ such that $d_T(\mathcal{T}_g, p_t) \leq (\sqrt{3}+1)r_{\min}$ in Algorithm 2, as the attack can be easily achieved from p_e .

Proof. The proof is provided in Appendix E. \square

Theorem 5 gives the attack performance bounds of Algorithm 3, in terms of the attack path length (compared with Algorithm 2) and the attack activity ratio. In Section VI, we will illustrate the worst performance is hard to actually meet. Note that the core insight of Algorithm 3 lies in how to leverage the inertia property of R_v 's obstacle-avoidance behavior to make R_a more inactive, not in how to design the best attack move for R_a when it needs be active. Therefore, it can also be compared with other attack algorithms by replacing the [Line 9, 15] of Algorithm 3 with the attack move computed by other algorithms, and the similar conclusions to Theorem 5 still hold.

E. Attack against Holonomic Robots

For holonomic robots, the attack performance (results of Theorems 4-5) for R_a is the same under Algorithm 2 and 3. The major difference is that the motions of holonomic robots in two orthogonal directions are independent and involve no coupling constraints, and there is no need to compute their orientations, making learning the obstacle-avoidance mechanism easier for R_a . Therefore, attacks against holonomic robots with omnidirectional moving ability are not subject to the limitations of Theorem 3, i.e., the preset trap is arbitrary. However, due to the same reason, a stronger moving ability for R_a is required to move to its optimal attack position.

VI. SIMULATIONS

In this section, we model both non-holonomic and holonomic robots as simulation objects. Specifically, we adopt the popular dynamic window approach (DWA) [59], [60] and artificial potential method (APM) [32] as the obstacle-avoidance mechanism of the two kinds of robots, respectively. Our evaluation focuses on two aspects: effectiveness and efficiency. For better illustrating and depicting the attack process as detailed as possible in a square figure, we set the initial positions of R_a , R_v , the trap, and the goal roughly on the four corners (other settings that meet the attack conditions exhibit similar results). First, the critical learning steps of the proposed attack framework are shown. Then, we illustrate the effectiveness of the proposed control designs by presenting

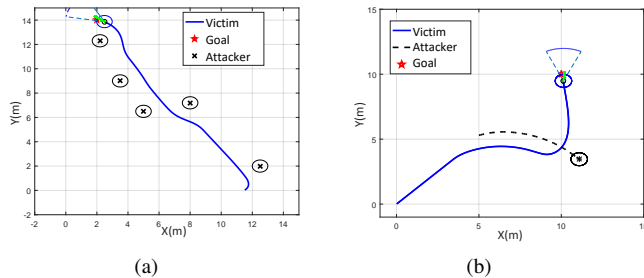


Fig. 7. (a) Intentional learning: R_a disguises as an obstacle to influence R_v 's running, and then collects the reaction data of R_v at 'x' positions consecutively. R_v moves from $(11.5, 0)$ to $(2, 14)$. (b) Simple attack: once R_a appears in (D, α) , it makes continuous impacts on R_v in one direction (here is to the right).

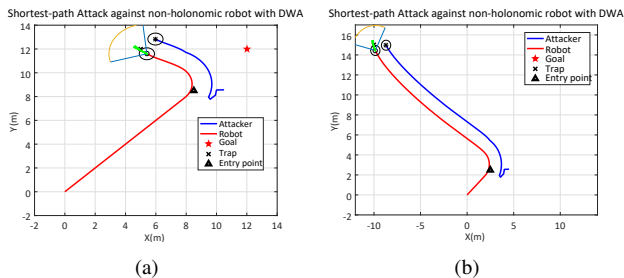


Fig. 8. Shortest-path attack against non-holonomic robot. The obstacle-avoidance algorithm of R_v is DWA. (a) The preset trap locates in $(5, 12)$. Attack iteration time is 89 steps, and the path length after being attacked is 5.52m. (b) The preset trap locates in $(-10, 15)$. Attack iteration time is 296 steps, and the path length after being attacked is 18.35m.

different attack scenarios and evaluating the attack costs. Finally, detailed comparisons with other works are provided.

A. Learning Phase

Fig. 7(a) shows that R_a collects a series of Q_{in} and Q_{out} by sequential "intentional learning". It is feasible to regress the obstacle-avoidance algorithm using the data, when no prior information of that is available. Fig. 7(b) shows a simple and rough attack: once R_a appears in (D, α) , it predicts R_v 's next move, and runs in the predicted direction with faster speed and repeats this process. As expected, R_v should keep avoiding R_a all the time. However, this attack cannot proceed consistently. We conclude the leading cause lies in two parts: i) The control inputs are not well-designed by considering where the next (sub-)optimal attack position is; ii) Each prediction will produce certain inaccuracy, which is cumulated to influence the attack effect in this case. Next, we present the results of the proposed attack algorithms. By comparison, the effectiveness of the algorithms is exhibited, remedying the deficiency of the former one.

B. Attack Phase

Basic setup: The goal position of R_v is set as $(12, 12)$. For a fair comparison, the same two cases for all attack strategies are designed where the trap is set as $(5, 12)$ and $(-10, 15)$, respectively. The traps locates in area \mathcal{A}_1 (defined in Fig. 4), satisfying the conditions in Theorem 3. Fig. 8 shows that the

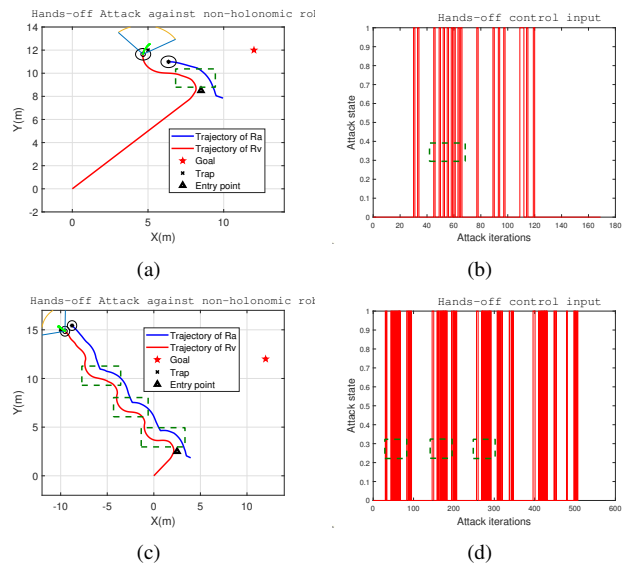


Fig. 9. Illustration of the hands-off attack against non-holonomic robot. The obstacle-avoidance algorithm of R_v is DWA. In hands-off control input, the state 1 means R_a is active while state 0 means R_a stays still. The marked parts with green rectangles mean the attack move is intensive. (a) and (b): The preset trap locates in $(5, 12)$. Attack horizon is 169 steps, R_a is active only for 20 steps, and the path length after being attacked is 6.56m. (c) and (d): The preset trap locates in $(-10, 15)$. Attack horizon is 509 steps, R_a is active only for 78 steps, and the path length after being attacked is 20.43m.

shortest-path attack strategy against a non-holonomic robot is applied. Fig. 9 shows that the hands-off attack strategy against a non-holonomic robot is applied. Examples of the holonomic robot are presented in Fig. 10.

Results analysis: In terms of path cost, from Fig. 8 we can observe that the trajectory of R_v is near to \mathcal{T}_a by the shortest-path attack, and the trajectory of R_v by hands-off attack twists and turns a little more, as shown in Fig. 9. Therefore, the former attack strategy is better in the sense of attack path length. For example, it is 5.52m in Fig. 8(a) while 6.56m in Fig. 9(a), consistent with the conclusion in Theorem 5. However, if we focus on the active attack time, it is found that the small sacrifice of path length largely saves the attack times for R_a by hands-off attack. As shown in Fig. 9(b) and 9(d), R_a only needs to attack in part times of the whole process to implement the attack successfully. The marked parts with green rectangle show this part of trajectory twists and turns, meaning the attack moves in this period are intensive. The reason lies in that R_a needs to make sure that R_v moves towards the trap, not adjusting to the goal direction in time [Line 6-21, Algorithm 2]. Taking the case of trap $(-10, 15)$ as an example, by hands-off attack, the attack horizon is 509 steps and R_a is active only for 78 steps, consistent with Theorem 5.

For a holonomic robot R_v , note that its trajectory is not as smooth as that of a non-holonomic robot, i.e., the moving direction of R_v may suddenly change. Even though this property makes the movement of R_v more unconstrained, the response trajectory of R_v is not necessarily shorter than that of a non-holonomic robot, as we can see from Fig. 8(b) and Fig. 10(b). The reason is as follows. If the obstacle detection range of this obstacle-avoidance model is neglected, we can always obtain a corresponding obstacle position to make R_v

TABLE II
COMPARISONS WITH REPRESENTATIVE WORKS OF HERDING PROBLEMS

Works	Dynamic model of target robot ¹	Self-goal consideration ²	Model is not priorly known ³	Make target robot go preset position	Required number of active robots
[61]	potential function based			✓	multiple
[11]	potential function based		partially known	✓	multiple
[12]	nonlinear Lipschitz function		✓	✓	single
[62]	flocking model			not fixed	single
[63]	flocking model		✓	✓	multiple
Our work	majority of obstacle-avoidance algorithms	✓	✓	✓	single

¹For comparisons in a uniform framework, the herd robot in herding problem and the victim robot in our work are both referred as the target robot, the herder robot in herding problem and the attack robot in our work are both referred as the active robot. ²This factor indicates that whether the dynamic model of target robot contains an intrinsic goal position, i.e., the dynamics of the target robot is not only determined by the active robot, but also by its intrinsic goal position. ³This means whether the active robot knows the dynamic model of the target robot to design control strategies.

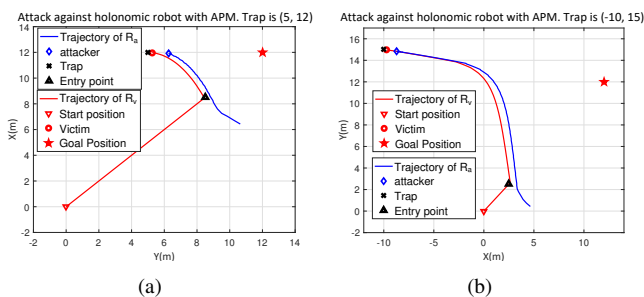


Fig. 10. Illustration of the shortest-path attack against holonomic robot. The obstacle-avoidance algorithm of R_v is APF. (a) The preset trap locates in (5, 12). And the path length after being attacked is 5.13m. (b) The preset trap locates in (-10, 15). And the path length after being attacked is 20.78m.

move to any desired position. Nevertheless, in our design which takes real limitations into consideration, the feasible positions of R_a to implement an attack are strictly constrained, formulated as (32d) or (29d) and (29e). Therefore, a desired next-step position may not be feasible, and we can only choose a position whose effect is closest to the desired position.

C. Comparisons with Other Works

The proposed attack shares some similar features with conventional pursuit-evasion problems (e.g., [7]–[9]) and herding problems (e.g., [10]–[12]), as they all utilize the interaction characteristic of the robots to achieve the specific tasks. However, it would be inappropriate to directly compare the method performance with these works, due to the major difference in their basic model formulation and application scenarios. For intuitive illustrations, the comparisons with some representative works are provided in Table II, which can be interpreted from the following three aspects.

- *Task scenario.* The proposed attack aims to drive the target robot into a preset trap position by utilizing the obstacle-avoidance mechanism. While in pursuit-evasion problems, the aim of the pursuers is to capture the evaders, which is usually turned to closely track the evaders or form an encirclement over the evader.

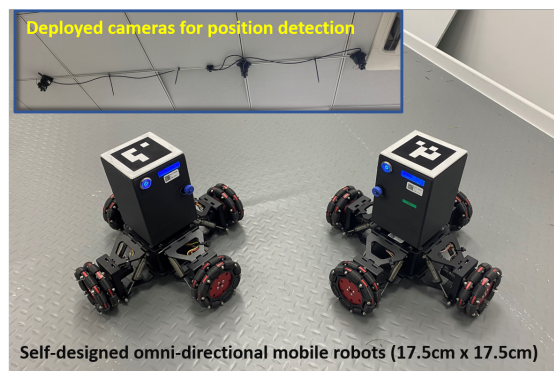


Fig. 11. The robot platform preview. Each robot is equipped with an unique code pattern on its top face for position detection. The position detection is performed by the multi-camera system deployed to the laboratory ceiling.

- *Model knowledge.* Our work focuses on learning the knowledge about the interaction mechanism of mobile robots and then utilizing the learned model to design a driving-to-trap attack, while most existing works rarely discuss the former issue about model knowledge, e.g., many herding problem works assume the interaction model of the robot is priorly known.
- *Model types:* The proposed attack is not tailored for a specific dynamic model of the victim robot. The dynamics of the robots in the pursuit-evasion is generally modeled as a multi-agent LTI systems, and in herding problems it is usually characterized by specific function forms (e.g., potential function), and only depends on the positions of the herding and target robots.

VII. EXPERIMENTS

A. Platform Description and Experiment Setup

To demonstrate the practical performance of the proposed attack, multiple experiments were conducted in our self-designed mobile robot platform [64]. The AprilTag visual system is adopted for the real-time localization of the robots. The control procedures based on the localization results are implemented by MATLAB in a VMWare ESXI virtual ma-

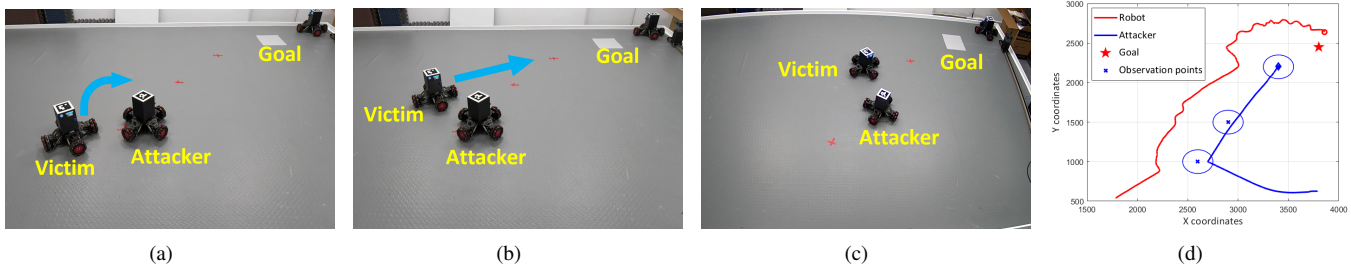


Fig. 12. Illustration of the intentional learning process. (a) R_v detects R_a and try to avoid it. (b) After R_a is off the detection range of R_v , R_v will continue approaching the goal. (c) R_a moves to the next observation point and makes impacts on R_v again. (d) The trajectories of the robots in this learning example.

chine, which is equipped with an Intel(R) Xeon(R) Gold 5220R CPU, 2.20G Hz processor and 16GB RAM.

We validate the result on a $5\text{ m} \times 3\text{ m}$ rectangular space in practice. Fig. 11 shows the used robots, which are with $17.5\text{ cm} \times 17.5\text{ cm} \times 20\text{ cm}$ volumes and designed in omnidirectional form. The robots are subject to the motion model (8), and their real-time positions are detected by the cameras deployed to the lab ceiling. The positions of the robot, goal, trap and other obstacles are represented by the coordinates of their geometric central points. Note that the unit of all motion states (e.g., position and speed) are described by the picture pixel hereafter, where 1 pixel in the calibrated picture is about 1.08 mm in the practical testbed.

For simplicity and intuitive comparison, the same initial position settings of the victim robot R_v , the attacker R_a , the goal p_g , and the preset trap p_t are used in different types of experiments. The initial positions of the victim robot and the attacker are $p_v(0) = [1800, 600]$ and $p_a(0) = [3800, 600]$, respectively. The goal and trap positions are $p_g = [3800, 2400]$ and $p_t = [1900, 2200]$, respectively. According to Definition 1, the entry point for the attacker is $p_e = [2670, 1373]$. The maximum velocity of the attacker and the victim robot are 400 pixel/s and 200 pixel/s. The obstacle-detection radius is set as $D = 600$ pixel. The robot is assumed to arrive at the goal or trap position, if $\|p_v - p_g\|_2 < 200$ or $\|p_v - p_t\|_2 < 200$.

B. Experiment Results

The first presented experiment is an illustration of the intentional learning stage, as shown in Fig. 12. In this experiment, the attacker is assigned three observation points $[2600, 1000]$, $[2900, 1500]$ and $[2900, 1500]$. Fig. 12(a)-Fig. 12(c) depicts the obstacle-avoidance process of the victim robot, when the attacker approaches it as an obstacle. The avoidance trajectory of the victim robot is observed by the attacker, and is used to construct the input-output pairs in the holonomic form of (21). Fig. 12(d) shows the complete trajectory evolution during this process. By conducting such intentional learning procedures in different positions, we obtain 200 groups of the input-output pairs to infer the goal position by the least squares method and learn the obstacle-avoidance mechanism by the SVR method. The inferred obstacle-detection radius and the goal position are $\hat{D} = 678$ pixel ($|\hat{D} - D| = 78$) and $\hat{p}_g = [3742, 2355]$ ($\|\hat{p}_g - p_g\|_2 = 73$), while the learned model achieves mean directional accuracy of 0.91 and root mean square error of

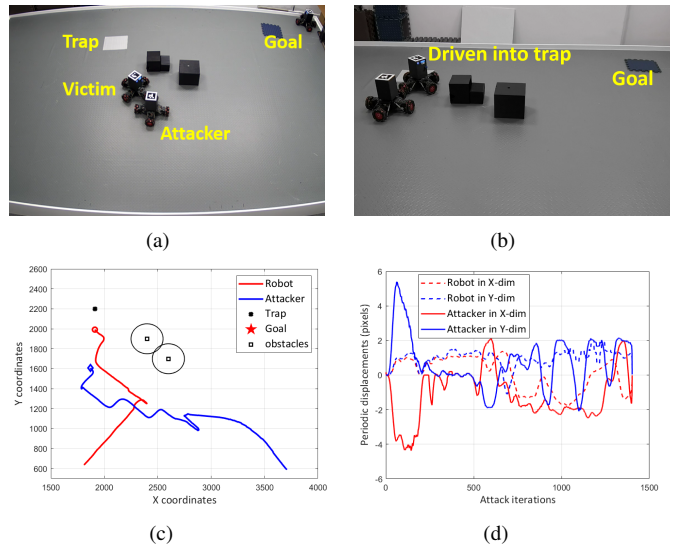


Fig. 13. Illustration of the shortest-path attack with other obstacles involved. (a) Snapshot during the attack process, where both R_a and R_v need to avoid the obstacles nearby. (b) Snapshot when R_v is successfully driven into the trap. (c) The trajectories of the robots, where the attack starts at step 490 and the ideal and actual attack path length are 1130 pixels and 1366 pixels, respectively. (d) The periodic displacements of the robots in two directions.

160.1 pixels, which are sufficient to support the following attack implementation.

Next, we focus on the validation of the proposed shortest-path and hands-off attack strategies based on the learned model. To better illustrate the performance and avoid repeating similar tests multiple times, we directly provide the results considering there are also other obstacles in the environment. Note that we use *periodic displacements* in a detection period of the cameras to describe the speed of the robots⁶.

Fig. 13 presents the results of the shortest-path attack, where the coordinates of the obstacles are $[2400, 1900]$ and $[2600, 1700]$, respectively. The snapshots of running process are shown in Fig. 13(a) and 13(b), while the trajectory and speed evolution of the robots are shown in Fig. 13(c) and 13(d). During the shortest-path attack, the attacker will consistently make moves around the victim robot. In this example, the attack state starts at step 490, and the ideal attack path

⁶Different from the simulation examples, the control period of the practical robots is not strictly a constant, but varies in a small range around the nominal value due to different computation burden and system noises. Therefore, we use the periodic displacements of the robots in two consecutive snapshots to plot the speed curve.

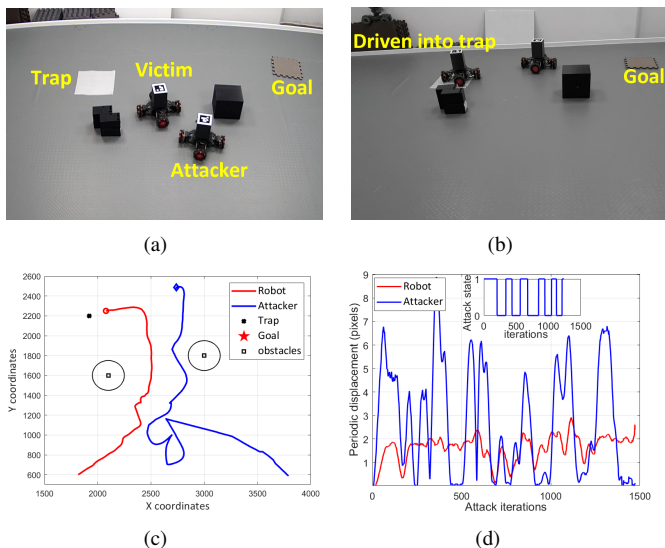


Fig. 14. Illustration of the hands-off attack with other obstacles involved. (a) Snapshot during the attack process, where both R_a and R_v needs to avoid the obstacles nearby. (b) Snapshot when R_v is successfully driven into the trap. (c) The trajectories of the robots, where the attack starts at step 309 and the total attack horizon is 1164 steps. (d) The resultant periodic displacements of the robots. The subfigure in the top right corner depicts the speed command state of R_a , where the active ratio of this example is 0.4356.

length is $\|[1900, 2200] - [2670, 1373]\|_2 = 1130$ pixels, while the practical path length is 1366 pixels. Note that this path deviation is mainly caused by the obstacles near the ideal path. Finally, we move to the example of the hands-off attack, where the coordinates of the obstacles are $[2400, 1900]$ and $[2600, 1700]$. Fig. 14 presents the results of the shortest-path attack, where the coordinates of the obstacles are $[2100, 1600]$ and $[3000, 1800]$, respectively. The attack starts at step 309 with a total attack horizon of 1164 steps. During the attack process, the attacker is only active for 507 steps in total, thus the active ratio of this example is 0.4356, which corresponds to the conclusion in Theorem 5. All the experiments demonstrate the effectiveness of the proposed attack. More experiment tests can be found in the attached video.

VIII. CONCLUSION

In this paper, the security problem of mobile robots is investigated. Different from most existing works, we propose a learning-based intelligent attack framework, where the attacker is able to learn certain dynamics of the target based on external observations, and then utilize it to accomplish its attack purpose in a more feasible and stealthier way. Specifically, without any prior information, the attacker is able to infer the victim robot's goal position and obstacle-detection area firstly. Then, the obstacle-avoidance mechanism is regressed by exploring the intrinsic characteristic of the mechanism and dynamically collecting reliable data in trials. Furthermore, two kinds of efficient control strategies for short path and high concealment attack objectives are designed, respectively. The feasibility analysis of the attacks and their performance bounds are provided, and the conditions for a successful attack implementation are proved. Extensive simulations and real-life experiments confirm the effectiveness of the proposed intelligent attack framework.

There are still many open issues that require further investigations. For example, we mainly focus on attack design in this paper, without more detailed consideration of defense for the victim robot. How to constitute an integrated framework containing both attack and defense needs further investigation. Meanwhile, the scenario considered in this paper is relatively simple, and applying the idea to more complicated scenarios is quite meaningful, like multi-robot coordination tasks. More generally, questions like what other dynamics information can be learned from external observation and what sophisticated attacks can be designed are also worth further exploration.

ACKNOWLEDGEMENT

The authors would like to thank Xuda Ding and Zitong Wang for their help in the attack experiments.

APPENDIX

A. Proof of Theorem 1

Proof. First, we prove that the trajectory can be approximated accurately in the asymptotic sense. Recalling $y_{l,j} = P_l^T \tilde{x}_{l,j} + \eta_{l,j}$ and the trajectory $\mathcal{T}_r^{(l)}$ is a straight line, thus the coefficient vector P_l is two-dimensional. For simple expressions, the variables are organized as $X_l = [\tilde{x}_{l,1}, \tilde{x}_{l,2}, \dots, \tilde{x}_{l,n_t}]^T$, $Y_l = [y_{l,1}, y_{l,2}, \dots, y_{l,n_t}]^T$ and $\Gamma_l = [\eta_{l,1}, \eta_{l,2}, \dots, \eta_{l,n_t}]^T$. Then, the problem is transformed to solve

$$\min_{P_l} \|Y_l - \tilde{X}_l P_l\|_2^2, \quad (46)$$

where its least square solution and error vector are given by

$$\hat{P}_l = (\tilde{X}_l^T \tilde{X}_l)^{-1} \tilde{X}_l^T Y_l, \quad (47)$$

$$E_l = \hat{P}_l - P_l = (\tilde{X}_l^T \tilde{X}_l)^{-1} \tilde{X}_l^T \Gamma_l, \quad (48)$$

Note that the trajectory is limited and each element in X_l is bounded, and one has $\|\tilde{X}_l^T \tilde{X}_l\|_2 = \mathcal{O}(n_t)$ and $\|(\tilde{X}_l^T \tilde{X}_l)^{-1}\|_2 = \mathcal{O}(1/n_t)$. Then, denote the element with largest absolute value in X_l as \tilde{x}_{\max} , and one has

$$\begin{cases} \mathbb{E} \left\{ \frac{[\tilde{X}_l^T \Gamma_l]_{ij}}{n_t} \right\} = \frac{1}{n_t} \sum_{n'_t=1}^{n_t} x_{n'_t}^i \mathbb{E}[\eta_{n'_t}^j] = 0, \\ \mathbb{D} \left\{ \frac{[\tilde{X}_l^T \Gamma_l]_{ij}}{n_t} \right\} = \sum_{n'_t=1}^{n_t} \left(\frac{[\tilde{X}_l]_{n'_t i}}{n_t} \right)^2 \sigma^2 \leq \frac{x_{\max}^2 \sigma^2}{n_t}. \end{cases} \quad (49)$$

By the famous Chebyshev inequality, given arbitrary $\epsilon > 0$, one has

$$\Pr \left\{ \left| \frac{[\tilde{X}_l^T \Gamma_l]_{ij}}{n_t} \right| < \epsilon \right\} \geq 1 - \frac{\mathbb{D}[\frac{[\tilde{X}_l^T \Gamma_l]_{ij}}{n_t}]}{\epsilon^2} \geq 1 - \frac{x_{\max}^2 \sigma^2}{n_t \epsilon^2}. \quad (50)$$

Let $\epsilon = (n_t)^{\frac{1}{4}}$ and substitute it into (50), and one infers that

$$\lim_{n_t \rightarrow \infty} \Pr\{\|E_l\|_2 = 0\} = 1. \quad (51)$$

Since p_g locates on the noise-free $\mathcal{T}_r^{(l)}$, it follows from (51) that $\lim_{n_t \rightarrow \infty} d_T(\mathcal{T}_r^{(l)}, p_g) = 0$, which proves the first statement.

Next, consider obtaining the goal p_g from the estimated trajectories $\{\mathcal{T}_r^{(l)}, l = 1, 2, \dots, n_z\}$. Let $\hat{P}_l = [\hat{a}_l, \hat{b}_l]^T$, $\hat{A} = [\hat{A}_0, -\mathbf{1}_{n_z}]$ ($\mathbf{1}_{n_z}$ represents all-one vector), $\hat{A}_0 =$

$[\tilde{a}_1, \dots, \tilde{a}_{n_z}]^\top$ and $\tilde{B} = [\tilde{b}_1, \dots, \tilde{b}_{n_z}]^\top$. Then, p_g can be obtained by solving

$$\min_{p_g} \|\tilde{A}p_g - \tilde{B}\|_2^2, \quad (52)$$

Like (46), the least square solution of (52) is given by

$$\hat{p}_g = (\tilde{A}^\top \tilde{A})^{-1} \tilde{A}^\top \tilde{B}. \quad (53)$$

Recall that the error vector $\tilde{A}p_g - \tilde{B}$ is also Gaussian according to (48). Therefore, the estimation error $\|\hat{p}_g - p_g\|_2$ will go to zero when $Z \rightarrow \infty$. The analysis is the same as that of \hat{P}_l and the details are omitted here. The proof is completed. \square

B. Proof of Theorem 2

Proof. First, we prove that $p_t \notin \mathcal{A}_{z1} \setminus \mathcal{A}_{z2}$ is a necessary condition by a limit performance analysis and logical deduction. The nature of the proposed attack to generate feasible p_a whose impact could offset the impact of p_g while lead R_v to p_t . In the proposed algorithms, this is done by keeping p_t and $\{p_a, p_g\}$ stay in different sides of $\mathcal{T}_m(p_v)$ after the attack begins, i.e.,

$$\begin{cases} I_T(\mathcal{T}_m(p_v), p_a) \cdot I_T(\mathcal{T}_m(p_v), p_g) > 0, \\ I_T(\mathcal{T}_m(p_v), p_a) \cdot I_T(\mathcal{T}_m(p_v), p_g) \cdot I_T(\mathcal{T}_m(p_v), p_t) < 0. \end{cases} \quad (54)$$

In the extreme case where R_v circumvents the obstacle with minimal curvature radius r_{\min} , if $p_t \in \mathcal{A}_u$, then there exists a certain moment k_c when $\mathcal{T}_m(p_v)$ is parallel with \mathcal{T}_{l1} (or \mathcal{T}_{l2}). After k_c , p_a and p_g are not at the same side of $\mathcal{T}_m(p_v)$, i.e., (54) does not hold, indicating that the impact of p_a to offset the impact of p_g reversely change and the movement of R_v is determined by p_g . Then, it follows that R_a cannot impose desired impact on R_v and the proposed algorithms cannot work to achieve the attack. On the contrary, for $p_t \notin \mathcal{A}_u$, an attack trajectory, which satisfies (54) while does not meet the extreme obstacle-avoidance behavior indicated by r_{\min} , can always be found by Algorithm 2 and Algorithm 3.

Next, we prove the convergence of Algorithm 2 from the optimization perspective when . Note that Algorithm 2 can be seen as a kind of one-dimension search method, and iteratively solves the following problem

$$\mathbf{P}_3 : \min_{p_v} F(p_v) = \|p_t - p_v\|_2^2. \quad (55)$$

Apparently, the global optimal solution of \mathbf{P}_3 is $p_v = p_t$ and this solution is unique. Therefore, we need to prove that the sequence $\{p_v(k)\}$ produced by Algorithm 2 will converge to p_t as k goes to infinity.

Note that the iterative searching process is of the form

$$p_v(k+1) = p_v(k) + \lambda_k S_k, \quad (56)$$

where vector S_k is called the search direction, and $\lambda_k \geq 0$ is called the step size. Similar to classic gradient-descent method, Algorithm 2 is essentially updating the search direction and step size. The feasible choice of the search direction is determined by the movement of R_a . For simple expression, we denote the search procedures of Algorithm 2 (i.e., Line 7-15) by a mapping $\phi: \mathbb{R}^2 \rightarrow \mathbb{R}$. Specifically, ϕ is equivalent to the following composite mapping,

$$\phi = \arg \min_{p_a} \{\phi_0(S_k) : S_k = \hat{p}_v(p_a) - p_v(k), p_a \in \mathcal{A}_a^f\}, \quad (57)$$

where the inner mapping ϕ_0 represents the step of updating λ_k , and is given by

$$\phi_0 = \min_{\lambda} \{h(p_v(k) + \lambda S_k) : \lambda \geq 0, \lambda \|S_k\|_2 \leq \mu\}, \quad (58)$$

With the feasible attack set \mathcal{A}_a^f determined, $S_k = \hat{p}_v(p_a) - p_v(k)$ is a descent search direction of $F(p_v)$, i.e.,

$$S_k^\top \nabla F(p_v(k)) < 0. \quad (59)$$

Then, one infers that $d_{vt}(k+1) \leq d_{vt}(k)$ and

$$F(p_v(k+1)) \leq F(p_v(k)). \quad (60)$$

Combining the differentiability and convexity of $F(p_v)$, it follows that ϕ is a closed mapping when $p_v \neq p_t$, and $F(p_v)$ is a descent function about p_t and ϕ . By the convergence theorem of search algorithms (refer to Chapter 7 in [58]), the two conditions ensure the sequence $\{p_v(k)\}$ produced by ϕ will converge to p_t . The proof is completed. \square

C. Proof of Theorem 3

Proof. In essence, the motion control of a mobile robot is in discrete form, thus we consider formulating the problem using breadth traversal analysis. All the solutions of the problem are represented by a tree, where the initial attack position $p_a(a_s + 1)$ is the root node and a node in floor k' denotes the attack inputs at attack iteration k' .

First, we prove the existence of a feasible move in each iteration. A feasible move means R_v will move closer to p_t , which can be achieved by making R_a 's position satisfy

$$\begin{cases} p_a \in \mathcal{A}_a(p_v), \\ I_T(\mathcal{T}_m(p_v), p_a) \cdot I_T(\mathcal{T}_m(p_v), p_t) < 0. \end{cases} \quad (61)$$

Apparently, there are multiple choices of p_a in each iteration such that (61) holds, and the next step is to determine the best p_a to implement the attack.

Based on (29b), multiple attack inputs from $\{u_a : \|u_a(k')\|_2 \leq \mu\}$ at attack step k' are sampled. Suppose the number of sampling groups is n , for every two adjacent node $u_a^i(k')$ and $u_a^{i-1}(k')$, the deviation $\|u_a^i(k') - u_a^{i-1}(k')\|_2$ is the same. Then, we define the sub-node set of $u_a(k')$ as $S_n(u_a(k'))$, whose cardinal number is n . Due to the constraint (29d), R_a can not stay unmoved all the time. Besides, at iteration k' , $u_a(k'+1)$ is computed such that the distance $\hat{d}(k+1) = \|\hat{p}_v(k+1) - p_t\|_2 \leq d(k) = \|p_v(k) - p_t\|_2$. As a consequence of the two factors, it is deduced that the length H of $\mathbf{u}_{a,0:H}$ is finite. Denote the maximum attack depth as \bar{H} and construct a solution as

$$\tilde{\mathbf{u}}_{a,0:H} = \{\tilde{u}_a(1), \tilde{u}_a(2), \dots, \tilde{u}_a(H)\}, \quad (62)$$

where $\tilde{u}_a(k'+1) \in S_n(u_a(k'))$, $k' = 1, 2, \dots, H-1$. By the constraints (29d) and (29e), many sub-nodes of a node $u_a(k')$ are excluded in Algorithm 2. Therefore, the total number of all feasible solutions $n_f \ll n^{\bar{H}}$.

Given a sampling size n , let $\tilde{\mathbf{u}}_{a,0:H}^{*,n}$ be the best solution among n_f feasible solutions, and it is intuitive to have

$$C_s(\tilde{\mathbf{u}}_{a,0:H}^{*,n+1}) \leq C_s(\tilde{\mathbf{u}}_{a,0:H}^{*,n}), \quad (63)$$

which is monotonically decreasing towards C_s^* with n growing. Therefore, when n is large enough, there exists a $\tilde{\mathbf{u}}_{a,0:H}^{*,n+1}$ (not necessarily unique) such that $|C_s(\tilde{\mathbf{u}}_{a,0:H}^{*,n+1}) - C_s^*| \leq \varepsilon$. The proof is completed. \square

D. Proof of Theorem 4

Proof. We prove this result by two steps. First, supposing the reaction radius r of R_v keeps unchanged under an attack pattern of R_a , we establish the bounds of l_{path} in the situation. Then, we scale the value of r to obtain the final bounds.

Step 1: Establish the bounds with unchanged r .

First, consider that R_a attacks R_v by being at the same relative position with it. This process continues until the orientation of R_v is heading towards p_t , the path length of this process is denoted as l_{path1} . Then R_a moves along with R_v such that R_v goes straightforward to p_t . The path length is of this process is l_{path2} . The pattern is represented by Pattern 1, shown in Fig. 6(b), and the angle between the second line and \mathcal{T}_a is

$$\xi = \arcsin\left(\frac{r}{d_{te} - r}\right). \quad (64)$$

By the calculation formula for arc length, we obtain $l_{pathA1} = (\pi/2 + \xi)r$, and $l_{pathA2} = (d_{te} - r) \cos \xi$. Then we have

$$l_{pathA} = (\pi/2 + \xi - \cos \xi)r + d_{te} \cos \xi. \quad (65)$$

Next, consider another attack pattern such that R_v moves two circular arcs, and the end is tangent to the line \mathcal{T}_a . The pattern is represented by Pattern 2, shown in Fig. 6(c). By the geometrical representation, the length of the arc part R_v passed is computed as $\frac{7}{6}\pi r$, and the length of the straight segment part is $d_{te} - (1 + \sqrt{3})r$. Then, we obtain

$$l_{pathB} = \left(\frac{7}{6}\pi - 1 - \sqrt{3}\right)r + d_{te}. \quad (66)$$

Note that $d_{te} > (\sqrt{3} + 1)r$ and $0 < \xi < \arcsin \frac{\sqrt{3}}{3}$, then

$$\begin{aligned} l_{pathB} - l_{pathA} &= \left(\frac{2\pi}{3} - 1 - \sqrt{3} - \xi + \cos \xi\right)r + d_{te}(1 - \cos \xi) \\ &\geq \left(\frac{2\pi}{3} - \xi - \sqrt{3} \cos \xi\right)r > 0.16r > 0. \end{aligned} \quad (67)$$

(67) implicates $l_{pathB} > l_{pathA}$ always holds. In fact, if the reaction radius of R_v is unchanged, the length of R_v 's path is bounded by l_{pathA} and l_{pathB} , i.e.,

$$(\pi/2 + \xi - \cos \xi)r + d_{te} \cos \xi \leq l_{path} \leq \left(\frac{7}{6}\pi - 1 - \sqrt{3}\right)r + d_{te}. \quad (68)$$

Step 2: Scale r .

Given a $r \in [r_{\min}, r_{\max}]$, the path length is bounded by (68). Since the path length is monotonically increasing with r increasing, the minimum path length is obtained when $r = r_{\min}$ and the trajectory is Pattern 1. The maximum path length is obtained when $r = r_{\max}$ and the trajectory is Pattern 2. By the design of Algorithm 2, even though the reaction radius of R_v is time-varying, it is also bounded in $[r_{\min}, r_{\max}]$. Then, it is induced that the real path length is between the minimum and the maximum path length. Due to $C_s^* = d_{te}$, we have $(\pi/2 + \xi - \cos \xi)r_{\min} + d_{te}(\cos \xi - 1) \leq \bar{C}_s - C_s^* \leq \left(\frac{7}{6}\pi - 1 - \sqrt{3}\right)r_{\max}$. The proof is completed. \square

E. Proof of Theorem 5

Proof. The performance bounds of Algorithm 3 can be obtained by resorting to analyzing a relaxed version of Algorithm 2, where the R_a does not have to be in the obstacle detection area all the time. Once the attack begins, R_a does the same procedure of [Line 12-20, Algorithm 2] to move, and the next iteration R_a stays inactive. By alternately running the two operations (equivalent to one attack move in every two iterations), the attack can still be achieved with a longer attack horizon. Note that at every inactive state, R_a 's impact on R_v does not perish but only work a little weaker than continuing its attack, i.e., R_v will still move towards p_t . Therefore, the attack horizon $H \leq 2H_1$ in Algorithm 3, with the active attack period $\|\mathbf{u}_{a,0:H}\|_0 = 0.5H$.

Next, by further relaxing the attack mode such that R_v always stays inactive if R_a 's impact still works while its movement limit is not violated, then we have $\|\mathbf{u}_{a,0:H}\|_0 < 0.5H$. The proof is completed. \square

REFERENCES

- [1] H. Choi, W.-C. Lee, Y. Aafer, F. Fei, Z. Tu, X. Zhang, D. Xu, and X. Xinyan, "Detecting attacks against robotic vehicles: A control invariant approach," in *Proceedings of the 2018 ACM SIGSAC Conference on Computer and Communications Security*. ACM, 2018, pp. 801–816.
- [2] D. Ding, Q.-L. Han, Y. Xiang, X. Ge, and X.-M. Zhang, "A survey on security control and attack detection for industrial cyber-physical systems," *Neurocomputing*, vol. 275, pp. 1674–1683, 2018.
- [3] H. S. Sánchez, D. Rotondo, T. Escobet, V. Puig, and J. Quevedo, "Bibliographical review on cyber attacks from a control oriented perspective," *Annual Reviews in Control*, vol. 48, pp. 103–128, 2019.
- [4] A. Pandey, S. Pandey, and D. Parhi, "Mobile robot navigation and obstacle avoidance techniques: A review," *International Robotics and Automation Journal*, vol. 2, no. 3, p. 22, 2017.
- [5] F. Pasqualetti, A. Bicchi, and F. Bullo, "Consensus computation in unreliable networks: A system theoretic approach," *IEEE Transactions on Automatic Control*, vol. 57, no. 1, pp. 90–104, 2012.
- [6] F. Pasqualetti, F. Dörfler, and F. Bullo, "Attack detection and identification in cyber-physical systems," *IEEE Transactions on Automatic Control*, vol. 58, no. 11, pp. 2715–2729, 2013.
- [7] R. Vidal, O. Shakernia, H. J. Kim, D. H. Shim, and S. Sastry, "Probabilistic pursuit-evasion games: Theory, implementation, and experimental evaluation," *IEEE Transactions on Robotics and Automation*, vol. 18, no. 5, pp. 662–669, 2002.
- [8] A. Kolling and S. Carpin, "Pursuit-evasion on trees by robot teams," *IEEE Transactions on Robotics*, vol. 26, no. 1, pp. 32–47, 2009.
- [9] V. G. Lopez, F. L. Lewis, Y. Wan, E. N. Sanchez, and L. Fan, "Solutions for multiagent pursuit-evasion games on communication graphs: Finite-time capture and asymptotic behaviors," *IEEE Transactions on Automatic Control*, vol. 65, no. 5, pp. 1911–1923, 2020.
- [10] W. Lee and D. Kim, "Autonomous herding behaviors of multiple target steering robots," *Sensors*, vol. 17, no. 12, p. 2729, 2017.
- [11] A. Varava, K. Hang, D. Kragic, and F. T. Pokorny, "Herding by caging: A topological approach towards guiding moving agents via mobile robots," in *Robotics: Science and Systems*, 2017.
- [12] R. A. Licitra, Z. I. Bell, and W. E. Dixon, "Single-agent indirect herding of multiple targets with uncertain dynamics," *IEEE Transactions on Robotics*, vol. 35, no. 4, pp. 847–860, 2019.
- [13] A. Ratnoo and T. Shima, "Line-of-sight interceptor guidance for defending an aircraft," *Journal of Guidance, Control, and Dynamics*, vol. 34, no. 2, pp. 522–532, 2011.
- [14] M. S. Darup, A. Redder, and D. E. Quevedo, "Encrypted cooperative control based on structured feedback," *IEEE Control Systems Letters*, vol. 3, no. 1, pp. 37–42, 2018.
- [15] A. B. Alexandru and G. J. Pappas, "Encrypted LQG using labeled homomorphic encryption," in *10th ACM/IEEE International Conference on Cyber-Physical Systems*. ACM, 2019, pp. 129–140.
- [16] Y. Li, J. He, C. Chen, and X. Guan, "Learning-based intelligent attack against formation control with obstacle-avoidance," in *2019 American Control Conference*. IEEE, 2019, pp. 2690–2695.

- [17] Q. Zhu and T. Basar, "Game-theoretic methods for robustness, security, and resilience of cyberphysical control systems: Games-in-games principle for optimal cross-layer resilient control systems," *IEEE Control Systems Magazine*, vol. 35, no. 1, pp. 46–65, 2015.
- [18] Z. Feng and G. Hu, "Secure cooperative event-triggered control of linear multiagent systems under DoS attacks," *IEEE Transactions on Control Systems Technology*, vol. 28, no. 3, pp. 741–752, 2020.
- [19] R. Su, "Supervisor synthesis to thwart cyber attack with bounded sensor reading alterations," *Automatica*, vol. 94, pp. 35–44, 2018.
- [20] Y. H. Chang, Q. Hu, and C. J. Tomlin, "Secure estimation based Kalman filter for cyber-physical systems against sensor attacks," *Automatica*, vol. 95, pp. 399–412, 2018.
- [21] Z. Liu, W. Chen, H. Wang, Y.-H. Liu, Y. Shen, and X. Fu, "A self-repairing algorithm with optimal repair path for maintaining motion synchronization of mobile robot network," *IEEE Transactions on Systems, Man, and Cybernetics: Systems*, vol. 50, no. 3, pp. 815–828, 2020.
- [22] Z. Liu, H. Wang, L. Xu, Y.-H. Liu, J. Lu, and W. Chen, "A failure-tolerant approach to synchronous formation control of mobile robots under communication delays," in *IEEE International Conference on Robotics and Automation*. IEEE, 2018, pp. 1661–1666.
- [23] X. Dong, B. Yu, Z. Shi, and Y. Zhong, "Time-varying formation control for unmanned aerial vehicles: Theories and applications," *IEEE Transactions on Control Systems Technology*, vol. 23, no. 1, pp. 340–348, 2014.
- [24] X. Dong and G. Hu, "Time-varying formation tracking for linear multi-agent systems with multiple leaders," *IEEE Transactions on Automatic Control*, vol. 62, no. 7, pp. 3658–3664, 2017.
- [25] V. S. Chipade and D. Panagou, "Herding an adversarial attacker to a safe area for defending safety-critical infrastructure," in *2019 American Control Conference*. IEEE, 2019, pp. 1035–1041.
- [26] D. Silvestre, P. Rosa, J. P. Hespanha, and C. Silvestre, "Stochastic and deterministic fault detection for randomized gossip algorithms," *Automatica*, vol. 78, pp. 46–60, 2017.
- [27] Y. Dong, N. Gupta, and N. Chopra, "False data injection attacks in bilateral teleoperation systems," *IEEE Transactions on Control Systems Technology*, vol. 28, no. 3, pp. 1168–1176, 2019.
- [28] N. O. Tippenhauer, C. Pöpper, K. B. Rasmussen, and S. Capkun, "On the requirements for successful GPS spoofing attacks," in *18th ACM Conference on Computer and Communications Security*. ACM, 2011, pp. 75–86.
- [29] G. Bianchin, Y.-C. Liu, and F. Pasqualetti, "Secure navigation of robots in adversarial environments," *IEEE Control Systems Letters*, vol. 4, no. 1, pp. 1–6, 2019.
- [30] Y. Son, H. Shin, D. Kim, Y. Park, J. Noh, K. Choi, J. Choi, and Y. Kim, "Rocking drones with intentional sound noise on gyroscopic sensors," in *24th USENIX Security Symposium*, 2015, pp. 881–896.
- [31] S. Skorobogatov, "Local heating attacks on flash memory devices," in *IEEE International Workshop on Hardware-Oriented Security and Trust*. IEEE, 2009, pp. 1–6.
- [32] O. Khatib, "Real-time obstacle avoidance for manipulators and mobile robots," in *Autonomous Robot Vehicles*. Springer, 1986, pp. 396–404.
- [33] E. A. Merchán-Cruz and A. S. Morris, "Fuzzy-GA-based trajectory planner for robot manipulators sharing a common workspace," *IEEE Transactions on Robotics*, vol. 22, no. 4, pp. 613–624, 2006.
- [34] X. Li and B.-J. Choi, "Design of obstacle avoidance system for mobile robot using fuzzy logic systems," *International Journal of Smart Home*, vol. 7, no. 3, pp. 321–328, 2013.
- [35] H. Li, S. X. Yang, and M. L. Seto, "Neural-network-based path planning for a multirobot system with moving obstacles," *IEEE Transactions on Systems, Man, and Cybernetics, Part C (Applications and Reviews)*, vol. 39, no. 4, pp. 410–419, 2009.
- [36] C. Goerzen, Z. Kong, and B. Mettler, "A survey of motion planning algorithms from the perspective of autonomous UAV guidance," *Journal of Intelligent and Robotic Systems*, vol. 57, no. 1-4, p. 65, 2010.
- [37] M. Mohanan and A. Salgoankar, "A survey of robotic motion planning in dynamic environments," *Robotics and Autonomous Systems*, vol. 100, pp. 171–185, 2018.
- [38] C. Tam, R. Bucknall, and A. Greig, "Review of collision avoidance and path planning methods for ships in close range encounters," *The Journal of Navigation*, vol. 62, no. 3, pp. 455–476, 2009.
- [39] K. D. Listmann, M. V. Masalawala, and J. Adamy, "Consensus for formation control of nonholonomic mobile robots," in *IEEE International Conference on Robotics and Automation*. IEEE, 2009, pp. 3886–3891.
- [40] C. Samson, "Time-varying feedback stabilization of car-like wheeled mobile robots," *The International Journal of Robotics Research*, vol. 12, no. 1, pp. 55–64, 1993.
- [41] A. Astolfi, "Exponential stabilization of a wheeled mobile robot via discontinuous control," *Journal of Dynamic Systems, Measurement, and Control*, vol. 121, no. 1, pp. 121–126, 1999.
- [42] J. Chen, D. Sun, J. Yang, and H. Chen, "Leader-follower formation control of multiple nonholonomic mobile robots incorporating a receding-horizon scheme," *The International Journal of Robotics Research*, vol. 29, no. 6, pp. 727–747, 2010.
- [43] J. R. Lawton, R. W. Beard, and B. J. Young, "A decentralized approach to formation maneuvers," *IEEE Transactions on Robotics and Automation*, vol. 19, no. 6, pp. 933–941, 2003.
- [44] T. Hernández, A. Loria, E. Nuño, and E. Panteley, "Consensus-based formation control of nonholonomic robots without velocity measurements," in *2020 European Control Conference*. IEEE, 2020, pp. 674–679.
- [45] X. Zhu, J. Yi, H. Ding, and L. He, "Velocity obstacle based on vertical ellipse for multirobot collision avoidance," *Journal of Intelligent and Robotic Systems*, vol. 99, no. 1, pp. 183–208, 2020.
- [46] L. Jaillet and T. Siméon, "A PRM-based motion planner for dynamically changing environments," in *IEEE/RSJ International Conference on Intelligent Robots and Systems*. IEEE, 2004, pp. 1606–1611.
- [47] F. Large, C. Laugier, and Z. Shiller, "Navigation among moving obstacles using the NLVO: Principles and applications to intelligent vehicles," *Autonomous Robots*, vol. 19, no. 2, pp. 159–171, 2005.
- [48] D. H. Shim and S. Sastry, "An evasive maneuvering algorithm for UAVs in see-and-avoid situations," in *2007 American Control Conference*. IEEE, 2007, pp. 3886–3891.
- [49] N. E. Du Toit and J. W. Burdick, "Robot motion planning in dynamic uncertain environments," *IEEE Transactions on Robotics*, vol. 28, no. 1, pp. 101–115, 2011.
- [50] X. Lan and M. Schwager, "Planning periodic persistent monitoring trajectories for sensing robots in Gaussian random fields," in *IEEE International Conference on Robotics and Automation*. IEEE, 2013, pp. 2415–2420.
- [51] G. A. Hollinger and G. S. Sukhatme, "Sampling-based motion planning for robotic information gathering," in *Robotics: Science and Systems*, 2013.
- [52] F. Pukelsheim, "The three sigma rule," *The American Statistician*, vol. 48, no. 2, pp. 88–91, 1994.
- [53] J. Chen, T. Liu, and S. Shen, "Tracking a moving target in cluttered environments using a quadrotor," in *IEEE/RSJ International Conference on Intelligent Robots and Systems*. IEEE, 2016, pp. 446–453.
- [54] N. Cristianini and J. Shawe-Taylor, *An Introduction to Support Vector Machines and Other Kernel-based Learning Methods*. Cambridge University Press, 2000.
- [55] Y. Liu and R. Bucknall, "A survey of formation control and motion planning of multiple unmanned vehicles," *Robotica*, pp. 1–29, 2018.
- [56] M. Donkers, P. Tabuada, and W. Heemels, "Minimum attention control for linear systems," *Discrete Event Dynamic Systems*, vol. 24, no. 2, pp. 199–218, 2014.
- [57] M. Nagahara, D. E. Quevedo, and D. Nešić, "Maximum hands-off control: A paradigm of control effort minimization," *IEEE Transactions on Automatic Control*, vol. 61, no. 3, pp. 735–747, 2015.
- [58] E. K. Chong and S. H. Zak, *An Introduction to Optimization*. John Wiley & Sons, 2004.
- [59] D. Fox, W. Burgard, and S. Thrun, "The dynamic window approach to collision avoidance," *IEEE Robotics and Automation Magazine*, vol. 4, no. 1, pp. 23–33, 1997.
- [60] M. Seder and I. Petrovic, "Dynamic window based approach to mobile robot motion control in the presence of moving obstacles," in *IEEE International Conference on Robotics and Automation*. IEEE, 2007, pp. 1986–1991.
- [61] A. Pierson and M. Schwager, "Controlling noncooperative herds with robotic herders," *IEEE Transactions on Robotics*, vol. 34, no. 2, pp. 517–525, 2017.
- [62] A. A. Paranjape, S.-J. Chung, K. Kim, and D. H. Shim, "Robotic herding of a flock of birds using an unmanned aerial vehicle," *IEEE Transactions on Robotics*, vol. 34, no. 4, pp. 901–915, 2018.
- [63] V. S. Chipade and D. Panagou, "Multiagent planning and control for swarm herding in 2-D obstacle environments under bounded inputs," *IEEE Transactions on Robotics*, vol. 37, no. 6, pp. 1956–1972, 2021.
- [64] X. Ding, H. Wang, H. Li, H. Jiang, and J. He, "Robopheus: A virtual-physical interactive mobile robotic testbed," *arXiv preprint arXiv:2103.04391*, 2021.



Yushan Li (S'19) received the B.E. degree in School of Artificial Intelligence and Automation from Huazhong University of Science and Technology, Wuhan, China, in 2018. He is currently working toward the Ph.D. degree with the Department of Automation, Shanghai Jiaotong University, Shanghai, China. He is a member of Intelligent of Wireless Networking and Cooperative Control group. His research interests include robotics, security of cyber-physical system, and distributed computation and optimization in multi-agent networks.



Jianping He (SM'19) is currently an associate professor in the Department of Automation at Shanghai Jiao Tong University. He received the Ph.D. degree in control science and engineering from Zhejiang University, Hangzhou, China, in 2013, and had been a research fellow in the Department of Electrical and Computer Engineering at University of Victoria, Canada, from Dec. 2013 to Mar. 2017. His research interests mainly include the distributed learning, control and optimization, security and privacy in network systems.

Dr. He serves as an Associate Editor for IEEE Trans. Control of Network Systems, IEEE Open Journal of Vehicular Technology, and KSII Trans. Internet and Information Systems. He was also a Guest Editor of IEEE TAC, International Journal of Robust and Nonlinear Control, etc. He was the winner of Outstanding Thesis Award, Chinese Association of Automation, 2015. He received the best paper award from IEEE WCSP'17, the best conference paper award from IEEE PESGM'17, and was a finalist for the best student paper award from IEEE ICCA'17, and the finalist best conference paper award from IEEE VTC'20-FALL.



Cailian Chen (M'06) received the B. Eng. and M.Eng. degrees in Automatic Control from Yanshan University, P. R. China in 2000 and 2002, respectively, and the Ph.D. degree in Control and Systems from City University of Hong Kong, Hong Kong SAR in 2006. She has been with the Department of Automation, Shanghai Jiao Tong University since 2008. She is now a Distinguished Professor.

Prof. Chen's research interests include industrial wireless networks, computational intelligence and situation awareness, Internet of Vehicles. She has authored 3 research monographs and over 100 referred international journal papers. She is the inventor of more than 20 patents. Dr. Chen received the prestigious "IEEE Transactions on Fuzzy Systems Outstanding Paper Award" in 2008, and "Best Paper Award" of WCSP'17 and YAC'18. She won the Second Prize of National Natural Science Award from the State Council of China in 2018, First Prize of Natural Science Award from The Ministry of Education of China in 2006 and 2016, respectively, and First Prize of Technological Invention of Shanghai Municipal, China in 2017. She was honored "Changjiang Young Scholar" in 2015 and "National Outstanding Young Researcher" by NSF of China in 2020.

Prof. Chen has been actively involved in various professional services. She is a Distinguished Lecturer of IEEE VTS. She serves as the Deputy Editor for National Science Open, and an Associate Editor of IEEE Transactions on Vehicular Technology, IET Cyber-Physical Systems: Theory and Applications, and Peer-to-peer Networking and Applications (Springer). She also served as the TPC Chair of ISAS'19, the Symposium TPC Co-chair of IEEE Globecom 2016, and the Track Co-chair of VTC2016-fall and VTC2020-fall.



Xinping Guan (F'18) received the B.Sc. degree in Mathematics from Harbin Normal University, Harbin, China, in 1986, and the Ph.D. degree in Control Science and Engineering from Harbin Institute of Technology, Harbin, China, in 1999.

He is currently a Chair Professor with Shanghai Jiao Tong University, Shanghai, China, where he is the Dean of School of Electronic, Information and Electrical Engineering, and the Director of the Key Laboratory of Systems Control and Information Processing, Ministry of Education of China. Before that, he was the Professor and Dean of Electrical Engineering, Yanshan University, Qinhuangdao, China. Dr. Guan's current research interests include industrial cyber-physical systems, wireless networking and applications in smart factory, and underwater networks. He has authored and/or coauthored 5 research monographs, more than 270 papers in IEEE Transactions and other peer-reviewed journals, and numerous conference papers. As a Principal Investigator, he has finished/been working on many national key projects. He is the leader of the prestigious Innovative Research Team of the National Natural Science Foundation of China (NSFC).

Dr. Guan is an Executive Committee Member of Chinese Automation Association Council and the Chinese Artificial Intelligence Association Council. He received the First Prize of Natural Science Award from the Ministry of Education of China in both 2006 and 2016, and the Second Prize of the National Natural Science Award of China in both 2008 and 2018. He was a recipient of the "IEEE Transactions on Fuzzy Systems Outstanding Paper Award" in 2008. He is a "National Outstanding Youth" honored by NSF of China, "Changjiang Scholar" by the Ministry of Education of China and "State-level Scholar" of "New Century Bai Qianwan Talent Program" of China.